LITERATURE REVIEW

White structure flaking (WSF) in wind turbine gearbox bearings: effects of 'butterflies' and white etching cracks (WECs)

M.-H. Evans*

The actual service life of wind turbine gearboxes is often well below the desired 20 years. One of the prevalent failure modes in gearbox bearing raceways is white structure flaking (WSF) by the formation of butterflies and white etching cracks with associated microstructural change called white etching areas. Despite these failures having been observed for two decades in various industries, the detailed reasons and mechanisms for their formation are not fully understood. In this review, white etching area formation mechanisms are discussed, specifically grain refinement, and effects of carbon/carbide in a range of bearing steels of widely differing carbon content. The review also highlights the severe transient, cyclic loading and tribochemical operating conditions of gearbox bearings and explains how these may act as drivers to produce WSF. Much previous research has focused on the detrimental effects of hydrogen, but other work suggests that hydrogen is not the only cause for WSF. Possible methods for preventing WSF are discussed, with attention paid to special steels such as high chromium steels, low carbon stainless nitrogen alloy steels and carbonitrided steels. Beneficial compressive residual stresses, surface coatings and enhanced lubrication and additive packages are shown to offer degrees of prevention, although the mechanisms leading to improvements are not fully understood.

Keywords: Butterflies, White etching, Brittle flaking, Microstructural change, Wind turbine gearbox, Rolling contact fatigue

This review is part of a special issue on 'Bearing steels' and is the winner of the 2011 Materials Literature Review Prize of the Institue of Materials, Minerals and Mining, which is administered by the Editorial Board of Materials Science and Technology

Introduction

The wind energy industry is experiencing an increasing interest from governments worldwide as they aim to meet their ambitious renewable energy targets. However, it is well established that the actual service life of wind turbine gearboxes is often well below the desired 20 years. Wind turbine gearboxes tend to fail predominately at several critical bearing locations, by the modes of micropitting, smearing and white structure flaking (WSF).[1] The 'L_{10} life' of a bearing characterises the rolling contact fatigue (RCF) life of a bearing for a given operating condition, at which statistically 90% of bearings survive. Normal RCF failures typically exceed the L_{10} life and eventually fail by spalling failure (flaking of the steel surface) which is unavoidable and will always eventually occur in bearings. Premature bearing failures in the form of WSF are another type of spalling which differs from the conventional subsurface slow material decay caused by RCF. The WSF type of flaking is not reserved to any one type of bearing, is unpredictable and has been observed to occur at as little as 1% of L_{10} life,[2] but more commonly at 5–10% of L_{10} life.[3–5] 'White structure' refers to the appearance of the altered microstructure when cross-sections are polished and etched with nital ($\sim$2% nitric acid in ethanol) or picral, and examined under reflected light, due to the non-etching nature of the altered material (Fig. 1).[6] White structure flaking (Fig. 2)[6] is caused by the formation of so called butterflies and white etching cracks (WECs) subsurface to a depth of just over 1 mm in the bearing raceways (Fig. 3) (gearbox model reconstructed from Ref. 7). White etching phenomena occur in many applications: on hard turned surfaces,[8–10] rail track surfaces,[11–15] as adiabatic shear bands in ordnance and machining processes,[16,17] and in rolling element bearings as white etching bands,[18–21] butterflies and WEC. The steel type varies widely between these applications: white etching layers (WELs) from hard turning,[9,10] adiabatic shear bands, white etching bands and butterflies/WEC have been found in standard bearing steel AISI 52100 for example, which has been used for over 100 years (*see* Tables 1 and 2). Rail steels are typically pearlitic steels (0·65–0·8 wt-%C) or bainitic steel (0·2–0·55 wt-%C) with manganese additions.[11,12,15] Surface WELs from hard turning are typically a few micrometres deep, with hardness of 900–1200 HV,[9,10] whereas WELs on rail tracks

National Centre for Advanced Tribology (nCATS), University of Southampton, UK

*Corresponding author, email martin_halfdan@hotmail.com

Published by Maney on behalf of the Institute
Received 4 May 2011; accepted 19 August 2011
DOI 10.1179/026708311X13135950699254

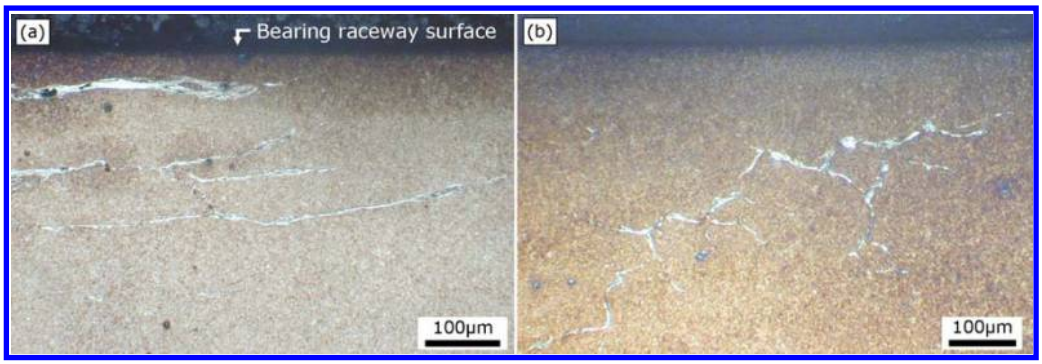

a parallel WEC; *b* branching network WEC

1 Optical images of axial sections through wind turbine inner ring bearing raceways showing WEC. 100CrMo7-3 bainite steel, double row spherical roller bearing, oil lubricated.[6] Copyright M.-H. Evans

form at the surface to a depth of ~100 μm, with a hardness of ~1200 HV.[11]

In bearing steels, white etching area (WEA) formation as butterflies and WECs occurs in martensitic through hardened steel,[23–40] bainite steel,[24] case hardened steel,[27,41–43] high chromium steel,[4,32,35,36,44] tungsten tool steel,[41] high speed tool steel,[31] graphite steel[28] and steel containing no carbides.[25] White etching area consists of almost equiaxed nanoferrite grains 10–100 nm in diameter,[23,24,27–30,38,40,45,46] is free of large carbides[21,23,25,28,29,40,46,47] and is supersaturated with carbon to varying weight percentages.[42,43] White etching area typically has hardness 30–50% higher than the matrix.[23,27,40]

Significant subsurface WEAs were reported several decades ago,[18,25,31,40,41] but it was not until just over a decade ago that WEC started to be widely reported.[1,3–5,24,28,30,32–39,41–44,48–58] The WEC has many synonyms: white structure, WEA, white banded flaking, irregular white etching area, unusual microstructural change, bright etched regions, exfoliation, peculiar microstructural change, flaking at early stage, white etching constituent (also WEC), subsurface initiated flaking, white etching bands, white layers, brittle flaking and hydrogen embrittlement. White structure occurs in wind turbine gearbox/main bearings,[1,5,48] hydrogen fuel cell system bearings,[38,55] marine POD drive bearings, automotive alternator, electromagnetic clutch, inclusion pulley, air conditioner compressor, water pump and driveline transmission bearings,[42,44,51,54,57,58] rolling members of toroidal continuously variable transmission,[59] aircraft turbine bearings,[41] crane lifting devices,[5] gears,[40] among others. However, despite these failures having been observed for two decades in various industries, their formation mechanisms and preventative solutions against them are either inadequate or not completely understood.

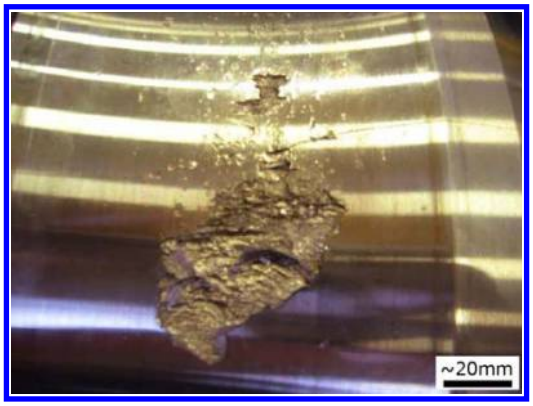

2 Optical image of material removal by WSF on wind turbine bearing inner raceway. Copyright M.-H. Evans

Gearboxes and their failure

Most wind turbines have a horizontal axis with a drive train incorporating a gearbox with ~15 bearings to step up the 20–35 rev min^{-1} rotor input to 1500–1800 rev min^{-1} (50–60 Hz) output for AC generation (Fig. 3). The high rate of growth in wind turbine size and capacity is resulting in more extreme operating conditions, resulting in more challenging design options, yet forced to incorporate materials which are already inadequate.[60] Hence, gearboxes are failing prematurely from 2 to 11 years,[48,61–65] where these failures often initiate at critical bearing locations, namely the planet bearings, intermediate shaft locating bearings and high speed locating bearings.[48,66] Gearbox replacement can cost up to £300k (2009);[63,67] therefore, their high failure rates are resulting in a higher cost for wind energy.

Gearbox operating conditions

Gearbox bearing failures are typically caused by the severe tribological environments and dynamic multiaxial loads faced.[1,68,69] For example, gearbox oil often overheats in service, contamination by particles and moisture is frequent and wind turbines are used all over the world in varying climates. One oil lubricates both gear and bearing contacts throughout widely differing speed and load operating conditions, leading to bearings often running in mixed and boundary lubrication regimes, and oils are often not completely changed out until 25 000–50 000 operating hours,[70] though online filtration is used and often oils are topped up with additives. An ever fluctuating torque is characteristic from the turbulent nature of wind (where for large wind turbines, this variation is relatively fast compared with rotational speed), resulting in accommodating drive train movement; hence, planet bearings for example are misaligned a number of times during a single revolution.[61] Gearbox bearings in general are subjected to various transients during operation such as wind gust loading, misalignment (i.e. excessive axial movement), sliding in between elements and race, inertia forces, braking loads, torque reversals from electrical grid fluctuations and severe vibrations.[71–73] Premature engagement of the wind turbine to the electrical grid results in accelerations and decelerations, overloading and instantaneous torque

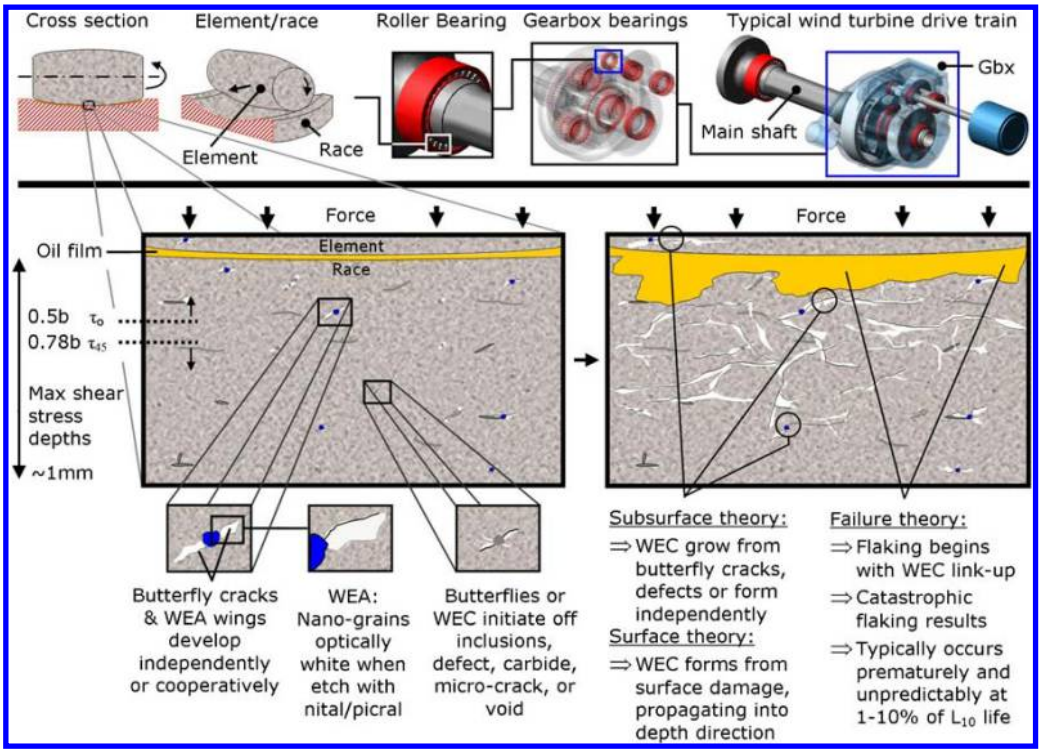

3 Butterflies and WECs leading to WSF failure in typical AISI 52100 martensitic through hardened steel. Typical gearbox configuration for 500 kW turbine with bearings highlighted in red. The first stage of the gearbox is a planetary system, where the sun pinion drives a parallel low speed shaft, driving an intermediate stage which in turn drives the high speed shaft. Wind turbine CAD model constructed from Ref. 7. To interpret the colour figure legends, the reader is referred to the web version of this article. Copyright M.-H. Evans

reversals, where turbines can typically experience ~3000 start-up/year with about five torque oscillations at each start, resulting in ~15 000 overloads/year.[60] Torque reversals can indirectly relocate load zones on bearings, where impact loading on sliding and misaligned elements cause peak stresses at certain element contact points.[1] Wind turbines often experience idling or long standstills either before electrical grid connection or during service, suffering tribological and loading problems at these times. The essence of the problem is that severe transient and tribological operating conditions in wind turbine gearbox bearings are still mostly unknown and thus bearings are not designed to sustain them.

Bearing steels and surface engineering

Bearing steels

Bearing steels must have high fatigue resistance against alternating shear stresses, resistance to wear and high elastic limit to prevent excessive deformation under load.[31] Tempering temperatures of common through hardened bearing steels, such as AISI 52100 and AISI 440C high carbon martensitic stainless steel (about 160–200°C), are well above the typical operating temperatures (90°C max.) of wind turbine gearboxes (though oil flash temperatures at asperity contacts will be significantly higher), and with their low cost, make them suitable for most bearing applications. Hardened bearing steels possess a complex microstructure: retained austenite, primary carbides, temper carbides and tempered martensite[74] (Fig. 4).[75] Non-metallic inclusions, voids, microcracks and carbide stringers can act as crack initiation points. With the increased cleanliness of steels, normal subsurface rolling contact initiated spalling from defects has decreased in occurrence, i.e. a tenfold life improvement from reducing oxygen content in steel from ~30 down to 5 ppm.[76,77] Maximum size of inclusions in steel has a large influence on the rolling contact fatigue life. For example, large rolling bearings made from bainitic steel typically have larger maximum inclusion sizes (about 50–80 μm) than

Table 1 Weight percentage composition of martensitic through hardened bearing steel 100Cr6, AISI/SAE-52100, JIS-SUJ2, EN31*

C	Mn	Si	P	S	Cr	Mo
0·98–1·10	0·25–0·45	0·15–0·35	0·025 max.	0·025 max.	1·30–1·60	0·00–0·10

Table 2 Mechanical properties of 100Cr6, AISI/SAE-52100, JIS-SUJ2, EN31 steels*

Yield limit (tension) $\sigma_{0·2}$,	Yield limit (compression) $\sigma_{0·2}$	Fracture toughness K_{1c}	Fatigue threshold stress intensity ΔK_{Th}	Vickers hardness
1220 MPa	2550 MPa	18 MPa $m^{1/2}$	4·5 MPa $m^{1/2}$	800±30 HV

*Reproduced from Ref. 23.

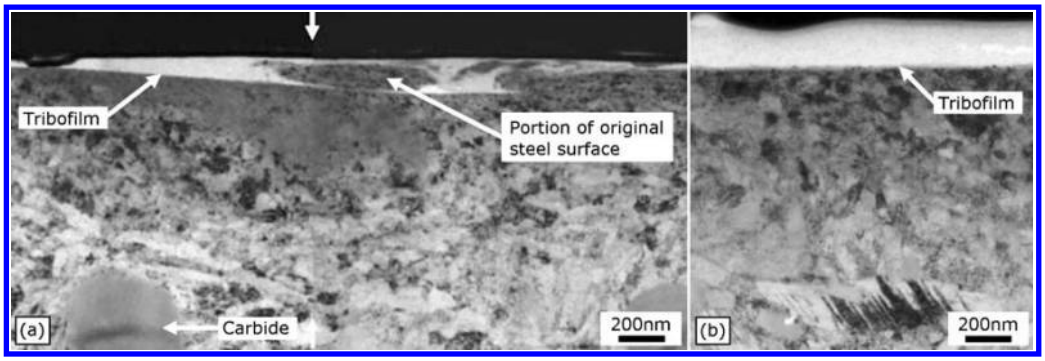

4 Transmission electron microscopy (TEM) cross-sections of wear track, where the ball rolled across the horizon of the image. *a* AISI 52100 steel showing tribofilm with a non-uniform thickness and structure, cracking, tribofilm penetration into the surface and surface particle detachment. White arrow indicates where two images are spliced together. *b* AISI 3310 case carburised steel (0·11 wt-%C, 0·53 wt-%Mn, 1·58 wt-%Cr and 3·5 wt-%Ni) showing uniform, thick and intact tribofilm of ~200 nm thickness with a sharp smooth interface with the matrix. Adapted from Ref. 75

AISI 52100 steel (about 10–15 μm). Since Murakami and co-workers[78] have shown by a fracture mechanic type approach that fatigue life is inversely proportional to the square root of the size of inclusions ($\sqrt{}$area parameter model), these large inclusions would adversely affect the fatigue life of large bainite bearings. The $\sqrt{}$area parameter model, however, does not take directly into account the orientation, morphology and location of the inclusions, which is discussed in the later butterfly initiation section. For WSF failures, however, some studies have shown that super clean grade steels have no or limited improvement in life. In through hardened bearing steel, fatigue properties increase with degree of hot working reduction;[79] however, it has been noted that heat treatment conditions do not significantly affect development of butterfly wing formations[24] (see later). Compared with carburised steel, through hardened steels have better dimensional stability and can sustain higher loads because of lower quantities of retained austenite, as austenite transforms to martensite under load with an associated volume increase.[80] Residual stress induced from manufacture differs between martensitic, bainitic and case hardened steels, which have tensile, compressive and high compressive residual stresses respectively from just below the surface to a depth of ~0·3 mm.[50] Compressive residual stresses subsurface in case hardened steels are beneficial in retarding crack development by decreasing the effective applied stress,[80] and are therefore used to negate tensile stresses in bearing rings that require tight interference fits.[81,82] Carburised steel which reduces bending stress in bearing outer rings due to compressive residual stresses,[42] and carbonitrided steel[3] can increase WSF life. Impurity atoms interact with dislocations and grain boundaries, trapping vacancies thus decreasing vacancy diffusion. Since carbides have been shown to dissolve as part of WEA formation, replacing these with more stable carbonitrides, Cr carbides[51] or transition metal carbides such as Mo[59] prolongs their decay. Additions of Si and Ni which strengthen the matrix and grain boundaries may also delay microstructural change.[37] AISI 52100 near surface material structure has a more coarse grain structure and spheroidal carbides typically an order of magnitude larger (about 1–2 μm compared with about 0·1–0·5 μm) than that of case carburised steel (Fig. 4).[83] AISI 52100 has been shown to be more susceptible to tribochemical wear than AISI 3310 case carburised steel (Fig. 4). Average carbon content in steels can influence WSF propensity. AISI 52100 has carbon content of 0·9–1·1 wt-%C, case hardened steels 0·1–0·3 wt-%C (0·65–1·1 wt-%C in the case hardened zone), whereas hardened steels containing 0·4–0·8 wt-%C show reduced occurrences of white structures.[5,25] AISI 440C high carbon martensitic stainless steel (1 wt-%C–17 wt-%Cr) is typically used in mildly corrosive environments. However, compared with AISI 52100, the dynamic load bearing capacity is lower and the steel contains coarse eutectic carbides which can act as crack initiators and chromium concentration sites.[80,84] Martensitic stainless steel ES1[51,84] has a lower carbon and chromium content than AISI 440C to suppress eutectic carbides and has a comparable hardness to AISI 52100. ES1 is alloyed with nitrogen which forms carbonitrides, strengthens the matrix and provides corrosion resistance, all the above enabling a tenfold increased WSF life compared with AISI 52100.[51] Martensitic stainless steel has a much lower hydrogen diffusivity rate than through hardened steel due to high contents of chromium, forming a passive film on its surface, which inhibits hydrogen diffusion and provides a strong hydrogen trap.[3,36] Additions of chromium which results in Cr carbide formation and chromium in the matrix prevent the generation of freshly exposed surface area during slip, preventing hydrogen generation and diffusion by passive chromium layer formation on the surface.[3,51]

Martensitic stainless steel exhibits a longer fatigue life under hydrogen testing,[85] generally (but not always) increasing WSF life compared with AISI 52100[3,32,44] by as much as fourfold,[51] where increases in chromium content to 13 wt-% can increase WSF life.[3,35,36] A hardness of >62 HRC in the ~1 mm surface zone is cited to increase WSF propensity due to the lattice strain and dislocation density being high, and the steel will temper as carbides will be in an unstable position, thereby the material will become unstable.[59] Although some residual austenite extends normal RCF life, in high amounts this increases WSF propensity and hence should be limited to 7–13%.[59]

Compressive residual stresses from rolling contact are induced in the circumferential[86–88] and axial[86,88] directions. The absence of high residual stresses in low load operation may increase WEC propensity. As it stands, carbonitriding, low carbon steel, high chromium steels and low carbon stainless nitrogen alloy steels may offer extended life, and research into tribofilm, compressive residual stress and carbide influence should be furthered.

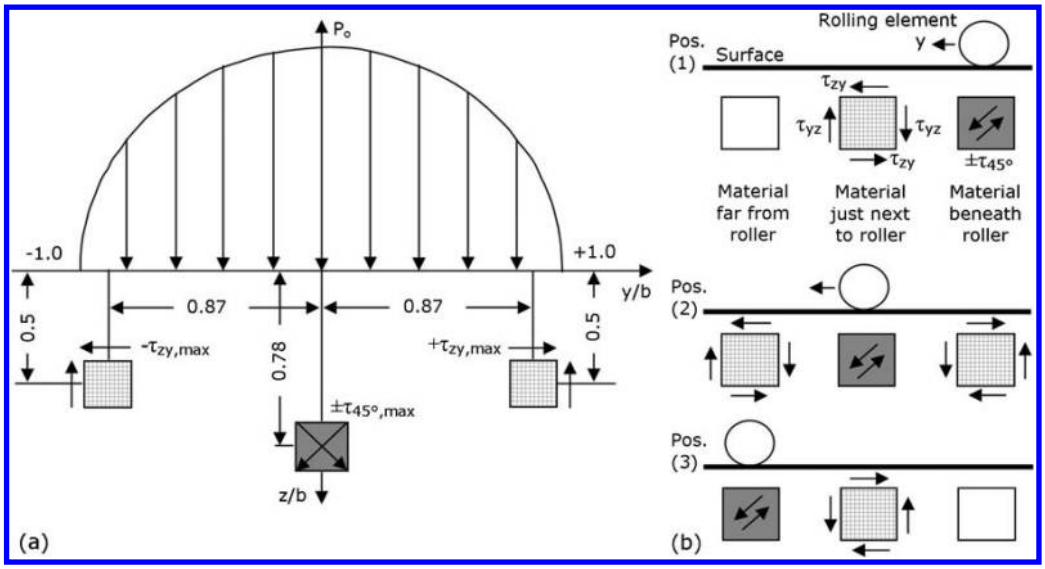

5 Line contact shear stresses present in material subsurface relative to Hertzian contact pressure P_o, where *b* is the semiwidth of the contact geometry in the rolling direction. *a* Maximum stressing according to orthogonal shear stress occurs at a depth of 0·5*b* and at a distance of $y = \pm 0{\cdot}87b$ from the centre of the contact area, which acts parallel and normal to the raceway, alternating in sign. The stress from unidirectional shear stress acts at a depth of 0·78*b* and in the centre of the contact area, forming an angle of ±45° with the tangent of the raceway. *b* Two-dimensional illustration of cyclic nature of subsurface shear stresses at one depth with three rolling element positions. Assumes steel with a Poisson's ratio of 0·3 and no friction in the contact. Adapted from Refs. 18 and 97 respectively

Surface engineering

An ~3 μm thick electroplated nickel film that diffuses into the raceway under rolling contact induced heat and stress,[43] and highly dense preformed trioctyl phosphate film,[32] prolong time until WSF by about fivefold[43] by prevention of hydrogen diffusion. Engineering surfaces with isotropic finishes and ~1 μm tungsten carbide incorporated amorphous hydrocarbon coated surfaces (WC/a-C:H) which reduce shear stress through sliding and prevent adhesive wear under high slip in boundary lubrication are cited.[1,89] Black oxide treatment on bearings prevents damage from smearing, increasing resistance to slippage and damage during alternating, low load conditions.[90] Black oxide is a mixed iron oxide produced in a dip solution, providing a soft 0·4–2 μm layer that increases film thickness, reduces traction coefficient and provides damping, being highly resistant to bending and stress,[89,91,92] offering protection against detrimental surface reactions from aggressive lubricants. Though black oxide wears off in operation, it typically prolongs WSF in wind turbine gearboxes; however, preventative mechanisms are not fully understood and the long term effects on gearbox components are unknown.

Cyclic rolling contact stresses

RCF is very different from classical fatigue. The state of stress in non-conformal contacts is complex and multiaxial. Although rolling bearings are not perfectly smooth and are lubricated, if oil film thickness is large compared with roughness, then Hertzian theory for determining contact pressure and subsurface stresses is still applicable with reasonable accuracy.[74] Actual contacts are rough and thus the stress field is more complex than a simple Hertzian type approach, as peak contact pressure will be experienced at raised asperities.[93] Hoop stresses (generally tensile) in bearing rings will be present from interference fits which reduce fatigue life,[81,82] and subsurface residual stresses are induced during overrolling.[19,86–88,94] An isotropic hydrostatic stress component from the weight of the material above the point concerned is present, which is absent in classical tension–compression or bending fatigue.[95] Contact stresses are compressive in three axes with differing values (principal stresses), which constantly change in direction during a stress cycle, resulting in the planes of maximum shear stress also changing.[95] The Lundberg–Palmgren theory[96] for bearing life ratings is based on twofold maximum orthogonal shear stress as the stress initiating material alteration, which acts parallel and normal to rolling direction, at $\pm 0{\cdot}87y/b$ and $0{\cdot}5z/b$ (Fig. 5).[97] Unidirectional shear stress acts at ±45° and at $0y/b$ and $0{\cdot}78z/b$. The WECs have been observed to propagate into the depth direction and form in a large range of depths (0–1·3 mm) and thus often do not correspond to the depths of calculated maximum shear stresses; hence, the stresses governing WEC are not yet clear.

The distortion energy hypothesis and unidirectional shear stress acting at 0·7–0·78*b* are thought to be the most robust ways of characterising RCF.[18] It is not thought that subsurface cracks develop at the instant of largest calculated material stressing in the load cycle, as this coincides when hydrostatic pressure is at a maximum, rather cracks probably develop at the relief phase of the load cycle (P=max. changing to P=0), when hydrostatic pressure is at its lowest.[18,26] The energy distortion hypothesis states that compressive residual stresses induced parallel to the raceway continually reduce material stressing; however, these residual stresses have little influence on the orthogonal shear stresses. Stress can be tensile in one of the three compressive principal stresses when hydrostatic pressure is deducted;[86] thus, tensile stress can act perpendicular to the direction of maximum compressive stress (i.e. into the depth direction). Tsushima[98] calculated shear stresses to be insufficient in high hardness steel for

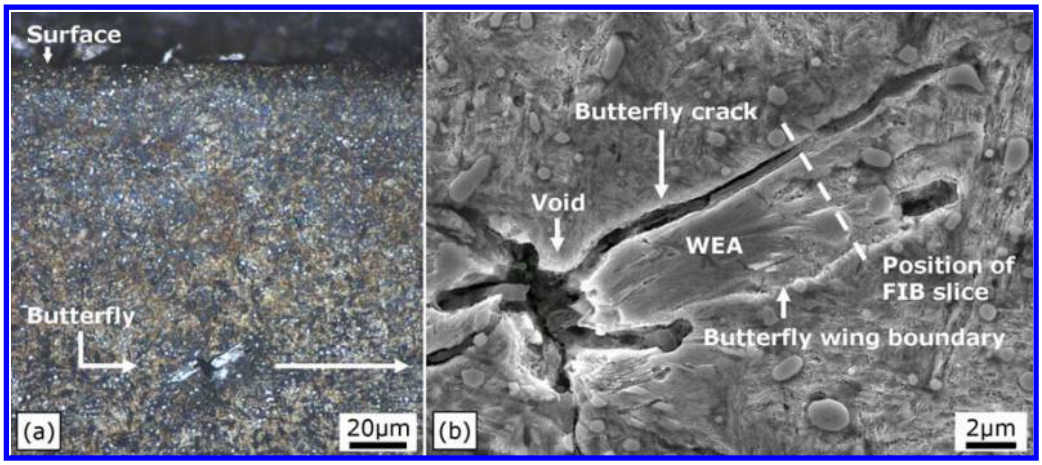

6 Circumferential section of 100Cr6 martensitically through hardened steel RCF roller specimen. *a* Optical image of butterfly, etched with 2% nital, where white structure can clearly be seen (image stitched together). *b* Scanning electron microscopy (SEM) image of butterfly in the as etched condition shown in *a*. Focused ion beam (FIB) cross-section is shown in Fig. 7. Copyright M.-H. Evans

crack development in the depth direction (under the weakening influence of hydrogen, see later section); thus, it is suggested that tensile stress can be large enough for crack development in the depth direction.

From the stresses induced by rolling contact, the material degradation due to normal RCF leading to a subsurface initiated fatigue spall in bearings can be described as a three stage process: shakedown, steady state elastic response and instability;[19,87,88,94,95] however, if white structure formation leading to flaking obeys this process, it must occur very prematurely in the third stage.

Butterflies and WEC

Butterflies

Butterflies are small cracks with altered microstructure wings, 10–250 μm in length, forming at depths of up to 1·5 mm[24,25] (Fig. 6) and are three-dimensional structures that sweep around their initiator[25,29,40] (*see* Fig. 7). Butterflies form at shallower depths in earlier periods of overrolling and at increasingly deeper depths with further overrolling, increasing temperature and increasing contact pressure.[26] Normal subsurface spalling is the formation of microcracks at non-metallic inclusions (with or without associated WEA butterfly wing formations) that eventually propagate to the surface causing spalling. What distinguishes WSF from normal subsurface spalling is that the cracks which may or may not propagate beyond the butterfly WEA wings may be of the WEC variety, forming WEC branching networks, not of the normal crack variety. Butterfly wings and cracks lie predominately at 30–50° (and 150–130°) to the direction of overrolling;[23,25–29,40,45] thus, unidirectional shear stress acting at $\pm 45°$ may be significant to their formation. The WEA wings consist of nanoferrite grains,[23,24,26–29,40,46] with smaller grains (10–50 nm) close to the cracks, and larger grains (50–100 nm) close to the butterfly boundary.[29]

Butterfly initiation

Butterflies initiate at defects, such as inclusions, voids,[28,29] microcracks,[25,28] grain boundaries,[41] large carbides,[27,40,41] carbide stringers and porosity.[26] For current bearing steels, sulphides, complex oxysulphides, oxides and titanium carbonitrides are typically present,[24] where butterflies preferentially form at oxides.[22,25] Figure 8 (Ref. 99) shows microstructurally altered material beside a Al_2O_3 inclusion, also observed by TEM around carbides.[40]

High quality bearing steels contain <10 ppm oxygen and therefore have few pure oxide inclusions,[100,101] but do contain duplex oxysulphides. Keeping the size of oxide inclusions as small as possible decreases propensity for butterfly initiated WEC.[59]

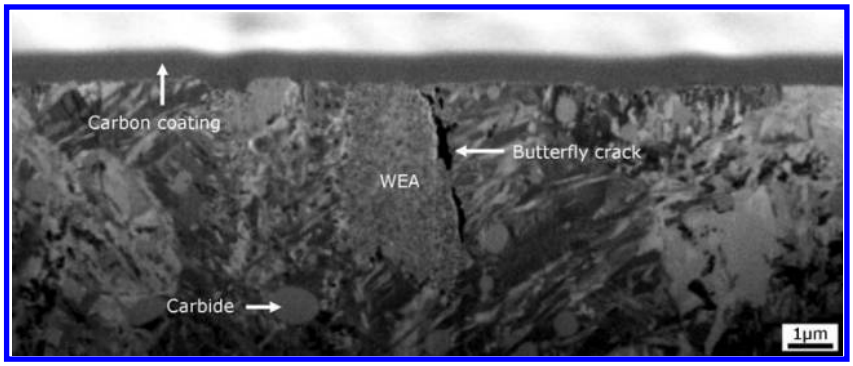

7 Focused ion beam (FIB) cross-section of butterfly wing in position highlighted by dotted line in Fig. 6. Carbon deposition acts as protection, Ga^+ source. The microstructural changes as nanograins forming the butterfly wing (WEA) are clearly distinguishable from the martensitic matrix. This highlights the three-dimensional nature of butterflies. Copyright M.-H. Evans and J. C. Walket

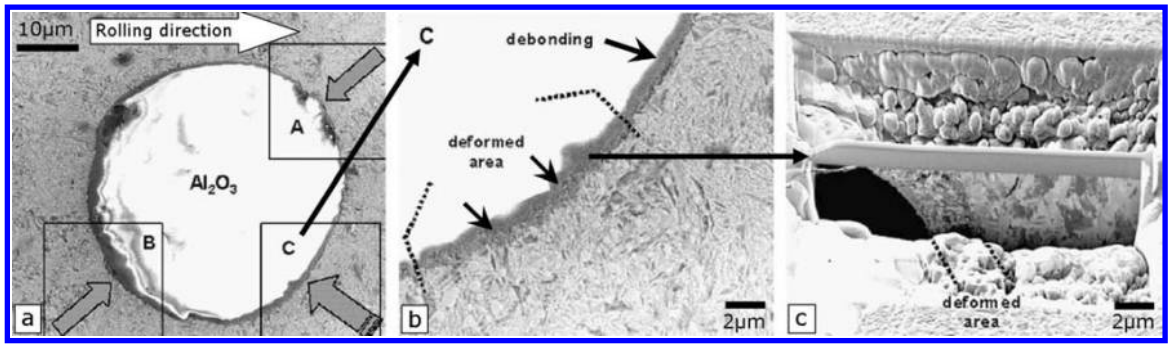

8 *a* SEM image of Al_2O_3 inclusion debonded at areas 'A' and 'B'. Area 'C' presents the region with deformed material at the inclusion/steel interface. *b* SEM image of detail 'C' showing the deformed interface region. *c* FIB cross-section of the lamella containing deformed region of fine granular structure along the inclusion interface. Depth=400 μm, contact pressure=2·6 GPa. Adapted from Ref. 99

Synchrotron X-ray microtomography revealed that orientation of inclusions with their associated cavities (gap between inclusion and matrix) influences the zone of material stressing,[102] where the presence of cavities may control the severity of inclusions.[103,104] Hashimoto *et al.*[104] showed that closing Al_2O_3 inclusion/matrix cavities in JIS-SUJ2 steel by hot isostatic pressing extended RCF crack initiation life. Calcium additions acting as deoxidisers in bearing steels have detrimental effects,[79] e.g. oxide inclusion composition affects butterfly formation and RCF life in the order of increasing severity as follows: SiO_2–Al_2O_3, Al_2O_3 and Al_2O_3–CaO.[79,103] Coefficients of thermal expansion (CTE) vary depending on inclusion type, where soft inclusions (e.g. MnS) have large CTE and hard inclusions (e.g. Al_2O_3) have small CTE compared with typical bearing steel microstructures; thus, compressive and tensile stresses respectively are induced surrounding the inclusion.[105] These induced residual stresses around inclusions are cited to enable initial crack growth relatively easily when combined with the overall cyclic shear stress field from rolling contact. These induced residual stresses will eventually reduce to zero with distance from the inclusion; however, cracks would still be able to grow from the overall cyclic shear stress field. In low temperature tempered (<400°C) bearing steels, cracks can initiate around non-metallic inclusions without externally applied stress[106] which could be prerequisites for butterfly formation.

Referring to Table 3, preferential butterfly formation at oxide parts of inclusions is due to the inclusion being hard and brittle, often displaying an incoherent interface with the matrix and debonding.[26,79,108] Softer, more ductile inclusions such as sulphides have a semicoherent interface with the steel matrix and can encapsulate non-metallic particles, so they do not act as stress concentrators.[22,40,79,109] Sulphides rarely initiate butterflies according to older literature,[25,40,79] on the other hand, in recent literature, MnS inclusions are said to initiate most butterflies.[110] Hence, the adhesion property and coherence between the inclusion and steel matrix is thought to be important in controlling the severity of the inclusion type.[23,25,27,40,79,111]

Butterfly initiated WSF from defects is likely to occur in the near surface zone of the total ~1 mm depth quoted. Thus, potential failure will be based on the probability of defects in this zone. Hence, an important distinction between small test samples/bearings and very large bearings in wind turbine gearboxes is the probability of a critical defect lying in this stressed zone.

Butterfly formation

Butterfly formation theory has been discussed extensively in early literature,[18,25,40,41,45,79,80,107,109,112,113] where areas of disagreement with the latest work,[23,26,29] are inclusion debonding, dislocation movement during plastic damage accumulation and which one forms first with regard to the butterfly crack and wing.[26]

The elastic modulus differences, differing CTE and/or the weak interfacial energy between the inclusion and matrix generate tensile and shear stresses in the locally surrounding matrix,[18,40,79,80] causing deformation and crack generation extending in the direction of the unidirectional shear stress, perhaps due to its influence.[18,107,113] Reversing rolling direction after a period of overrolling forms a second pair of wings in the symmetric orientation;[79] thus, microstructural change is not thermal, but stress induced.[40]

A microcrack being a prerequisite for the formation of butterflies has been postulated.[18,25,28,113] As WEA is hard, cracks may nucleate within prior formed WEA to relax localised stress during cycling, as it cannot plastically yield like the surrounding matrix,[40] or cracks may nucleate when a critical density of dislocations is reached,[107] though the later does not relate to other observations.[23,25,29,45,80] Österlund *et al.*[40] proposed successive grain nucleation out into the matrix, at the stress concentration zone on the interface of inclusion/matrix, this stress concentration zone propagating ahead of newly formed grains. It is thought that the butterfly initiation mechanism differs between different inclusion types. The latest theory of butterfly formation from hard

Table 3 Young's modulus *E* and hardness *H* of typical inclusions found in 100Cr6* (Young's modulus of 100Cr6 steel is 210 GPa with hardness of 8 GPa)

	Aluminium oxide	Titanium nitride	Spinel	Calcium aluminate I	Calcium aluminate II	Manganese sulphide
E/GPa	375	380	279	195	126	103
H/GPa	32·2	21·5	26·6	18·2	9·6	3·4

*The compositions of calcium aluminates I and II are $(Al_2O_3)_6$–(CaO) and $(Al_2O_3)_2$–(CaO). Adapted from Ref. 107.

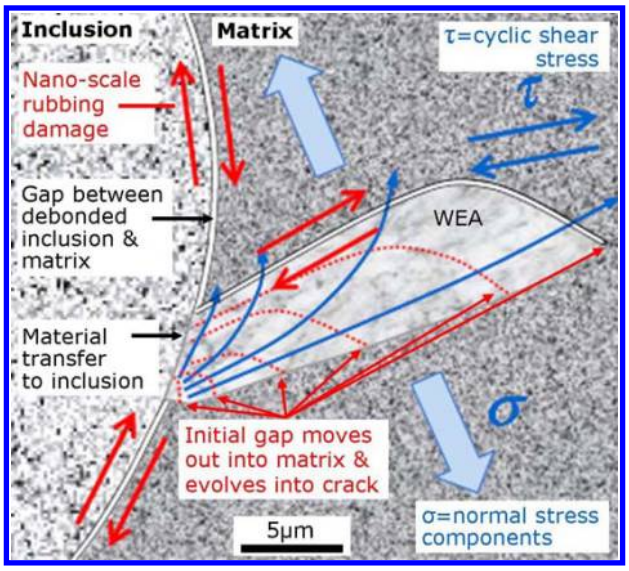

9 Schematic diagram of butterfly formation with overrolling from left to right. The gap from debonding of the oxide inclusion from the matrix is shown, as well as cyclic global stress field, which induces local rubbing between inclusion and matrix. The initial nanometre scale rubbing induces local shear damage accumulation and gradual material transfer across the gap and onto the inclusion surface. The initial gap (first dotted line) moves out into the steel matrix progressively from material transfer across crack faces and evolves into the main butterfly crack. Adapted with permission and courtesy of A. Grabulov[26]

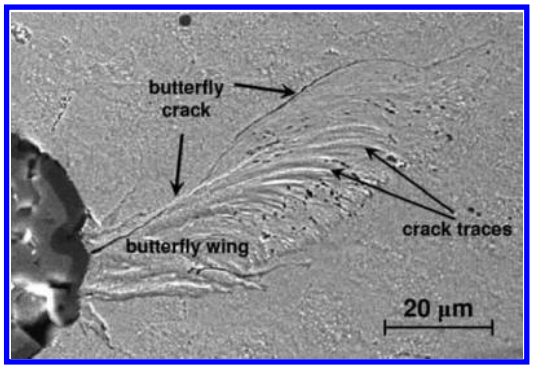

10 Image (SEM) of etched parallel section of AISI 52100 steel with overrolling left to right. Crack traces represent earlier positions of the butterfly crack. Image courtesy of A. Grabulov[26]

oxide type inclusions is cooperative growth of WEA wing and crack[26] (Fig. 9). Brückner *et al.*[110] proposed that butterflies initiating from MnS inclusions form first by the inclusion cracking through its length due to the subsurface stress field, with the crack subsequently extending into the matrix with cooperative WEA formation in the same way as that of oxide inclusions described in Fig. 9.

Butterfly propagation

The crack initiation stage is regarded to occupy ~99% of the total fatigue life in RCF,[100] only in the latest stage linear elastic fracture mechanics may be used to explain their further growth. Secondary microcracks[23] and voids[18,29,30,45,80] which lead to formation of cavities and pores[23,26,29] are also observed within WEA, where cavities may grow and coalesce into a central crack which propagates along localised shear planes at 45° into the matrix.[29] A gradual sidewise crack migration mechanism has been proposed[26] (Fig. 10); however, if the butterfly formation process did not follow that in Fig. 9, this would suggest that perhaps the main crack has repeatedly healed, or that the crack is moving due to diffusion, perhaps driven by compositional differences in carbon.

Butterfly wings typically increase in length with overrolling,[24] though not always.[28] With increased amounts of overrolling, the frequency of butterflies and size of the zone in which they generate increase,[25] and their growth is suppressed in these same areas by formation of dark etching area (damage by slip motions having occurred) by plastic deformation which reduces the stress concentration, hence suppressing microcrack formation.[25,80] Butterflies could be classed into two categories: those that do not propagate significantly thus not causing failure, and those that do propagate to a length which is critical, forming into cracks in the traditional sense or WEC (Fig. 11). Factors which could control whether butterflies are propagating or not are explored in later sections; however, in general, they can be thought of as stress transients above crack propagation thresholds (i.e. cracks repeatedly growing small amounts from higher than usual loading) and other influences which reduce thresholds for crack propagation such as weakening effect of hydrogen or tensile hoop stress.

Figure 12 shows a summary of butterfly characteristics and formation conditions.

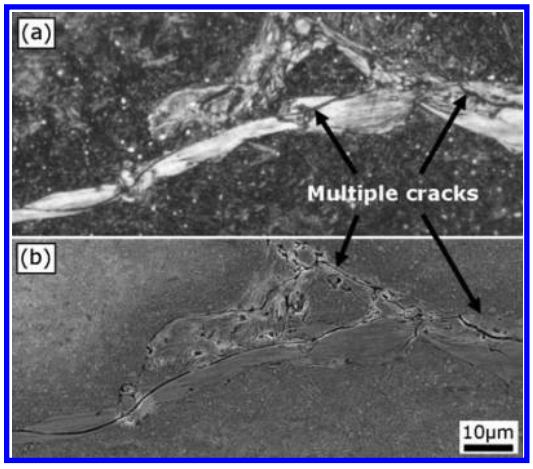

a optical and *b* SEW images of multiple cracks passing through a WEC in a wind turbine gearbox planet bearing.
11 Sample etched with 2%nital. Copyright M.-H. Evans.

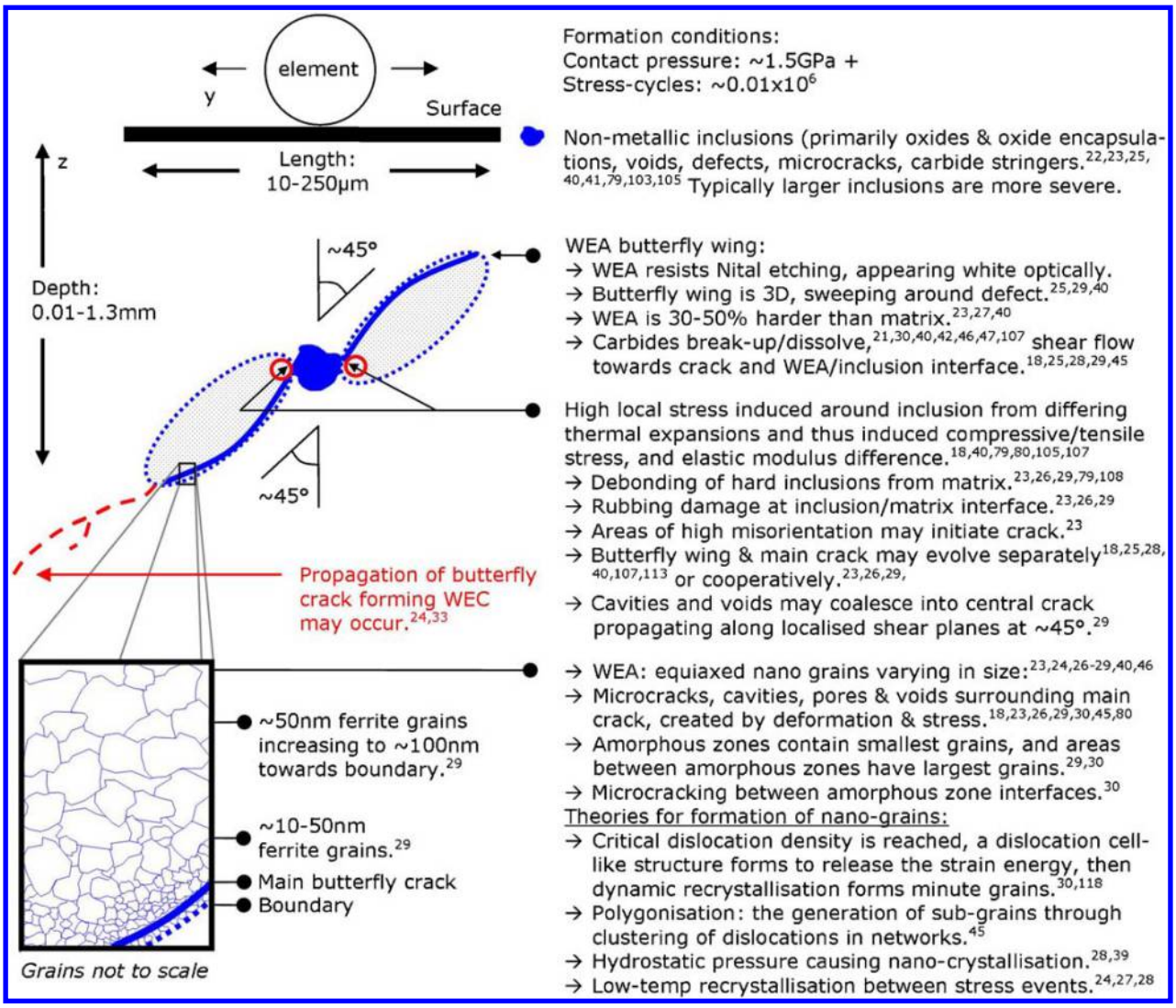

12 Butterfly characteristics and formation summary diagram. Overrolling plane of element across race is designated as *y*. Schematic is not to scale. Copyright M.-H. Evans

White etching cracks

White etching cracks are straight or branching crack systems with associated white structure borders, typically several millimetres in length when viewed as a two-dimensional section (Fig. 1).

White etching crack initiation, formation and propagation

White etching cracks probably initiate subsurface, but cross-sections are two-dimensional; thus, somewhere in the three-dimensional crack network, surface interaction could occur. Many authors have suggested that butterfly cracks continue to propagate forming WEC and flaking.[24,33,79] However, there is little experimental evidence to support that butterfly cracks propagate into WEC. A three-dimensional view could reveal butterfly initiators which would be otherwise missed. The WECs may also initiate from defects within the microstructure, or possibly independently.

Referring to Fig. 1, WECs do not form in directions specific to any maximum shear stresses, seemingly forming in either parallel or branching networks. In one study, two types of WECs were found to occur,[43]

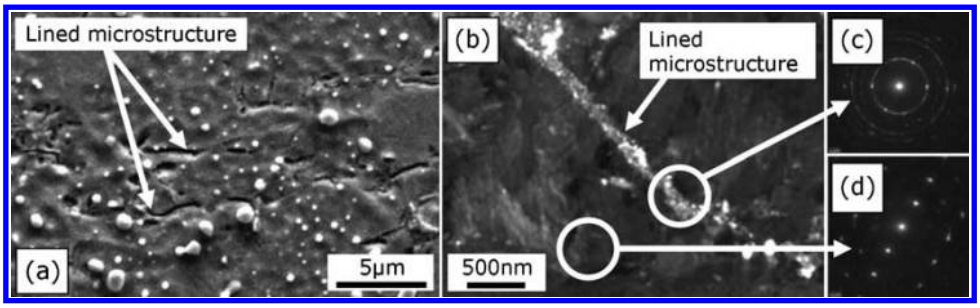

a SEM image of lined microstructure; *b* TEM image of lined microstructure; *c* diffraction pattern of lined microstructure revealing nanograined structure; *d* diffraction pattern on matrix beside lined microstructure

13 Microstructure close to flaking in hydrogen charged (0·4 ppm pretest) specimen which was a thrust bearing lower race. Cycles=3·4×10^7, max. contact pressure=3·1 GPa, rotational speed=1000 min^{-1}. Adapted from Ref. 38 with kind permission from the Japanese Society of Tribologists

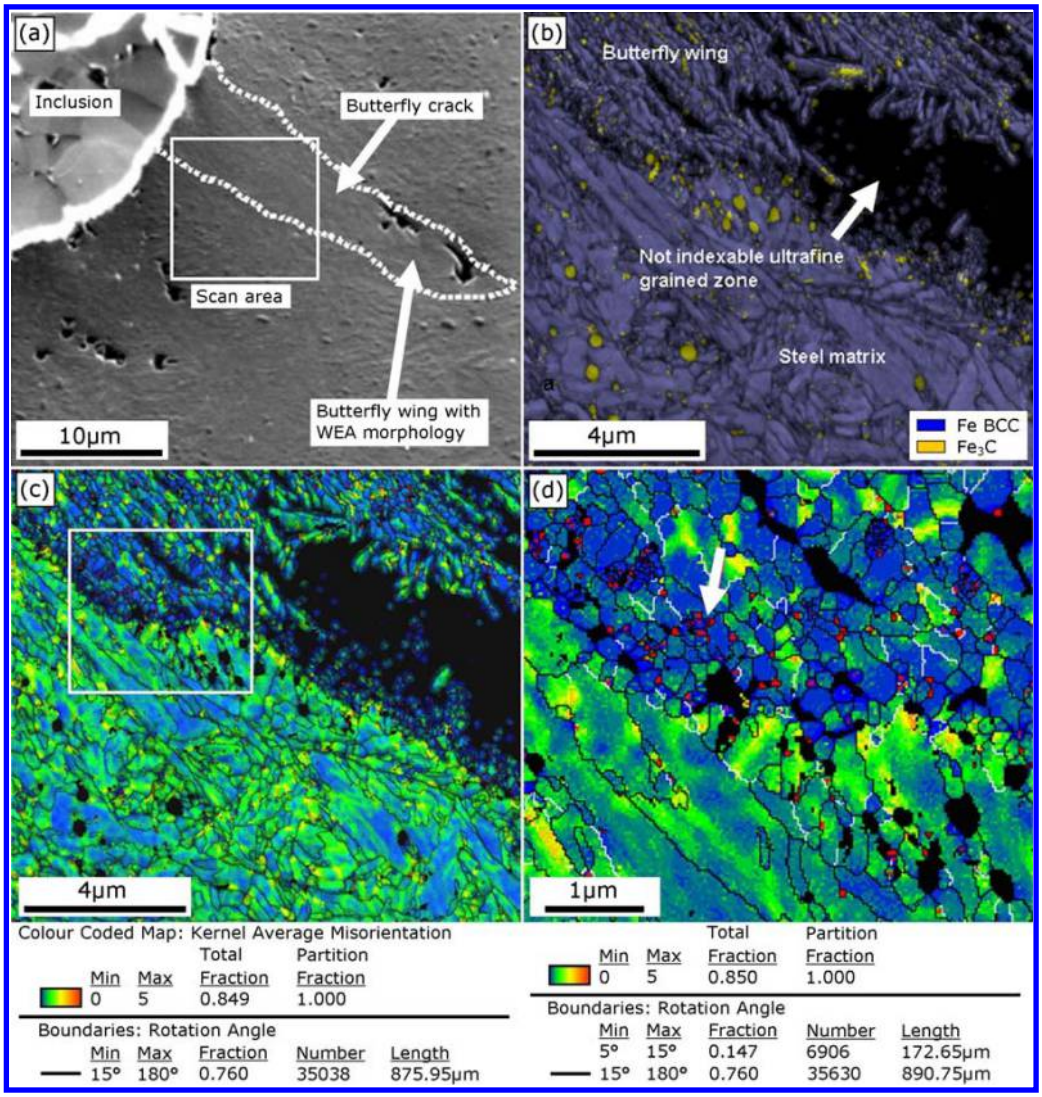

14 ***a*** **Image (SEM) of a butterfly wing around inclusion. The marked area (containing the steel matrix and the butterfly wing) marks the electron backscatter diffraction investigation location.** ***b*** **Automatic crystal orientation mapping: combined image quality and phase map showing the fine granular WEA and black unindexable area with grain diameter <50 nm, also displaying martensite (blue) and carbide (yellow) phases.** ***c*** **Colour coded kernel average misorientation (KAM) map displaying higher local misorientation in martensite matrix than in the butterfly wing.** ***d*** **Detailed view of box highlight from** ***c*** **consisting of fine grains with very low KAM inside the volume (blue) with a jump transition to the highest KAM next to the grain boundaries (red). Often such regions are situated next to the carbides (black). (To interpret the colour figure legends, the reader is referred to the web version of this article). Adapted from Ref. 99**

which often contain voids.[42] Cracks typically follow the white structure/matrix boundary or can pass through the white structure (Fig. 11).

In one study, thin cracks of 2–5 μm length without microstructural change are thought to be the prerequisite to WEC, forming by localised microscopic plastic deformation.[39] Other studies found thin lined microstructures only observable by SEM (Fig. 13*a*) consisting of ultrafine grained structures (Fig. 13*b*), which are thought to be the early formation of WEC.[38]

The WEC formation has mostly been attributed to hydrogen embrittlement,[3,4,30,32–38,43,44,51–55,57,100] with little mechanistic theories suggested. Some researchers supposed that microcracks and subsequent WEA formation generate everywhere just below the raceway, eventually uniting to result in flaking,[28,39] or that butterfly/independent crack initiation, subsequently grows into a crack system from multiaxial stresses, where WEA is perhaps just a consequence of material transfer by rubbing across crack faces.[33] Further research is clearly required to clarify mechanisms of WEC formation.

White structure formation mechanism

White structure has essentially the same morphology in butterfly wings and WEC. Some regions in butterfly wings consist of grains in diameter between 10 and 50 nm (Fig. 14*b*),[99] visible as black unindexible zones, which are usually associated with severe lattice distortions or increased dislocation density, and other coarser regions with well indexible body centred cubic grains, which were thought to originate from fragmented martensite lamellas. Figure 14*b* shows tempered martensitic phase and a second phase of precipitates (cementite) within the WEA, which was also observed in another study by dark field TEM;[40] in addition, inverse pole figure map showed that WEA exhibits no preferential crystallographic orientation.[23] Kernel average misorientation (KAM)

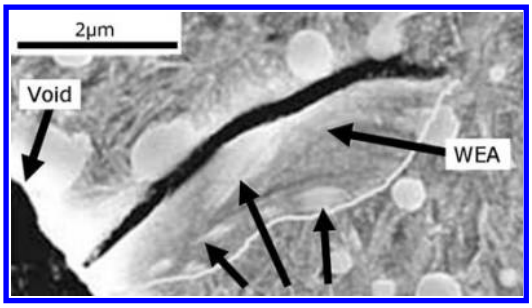

15 Secondary electron images of cementite dissolving into WEA towards microcrack in JIS-SUJ2 high chromium bearing steel prepared by powder metallurgy to contain voids. Black arrows point to apparent cementite dissolution. Thrust type rolling contact fatigue tester, cycles=5×10^5, max. contact pressure=3·92 GPa, depth=80 μm. Adapted from Ref. 115

maps (Fig. 14*c*) revealed that the local misorientation is smaller inside the WEA (does not exceed 0·7°) than in the matrix (average 0·88°), and comparison of grain size showed ~300 nm average grain diameter in WEA and ~900 nm in matrix. Areas of high local misorientation close to grain boundaries (red areas marked with arrow in Fig. 14*d*) may be crack initiation sites.

Diffraction patterns show WEA to be a body centred cubic structure,[23,29,30,38,49] which is a supersaturated cubic ferrite structure. Since carbon has poor solubility in ferrite, carbon must be accommodated by lattice defects such as vacancies, vacancy–carbon complexes, dislocation cores forming Cottrell atmosphere and the

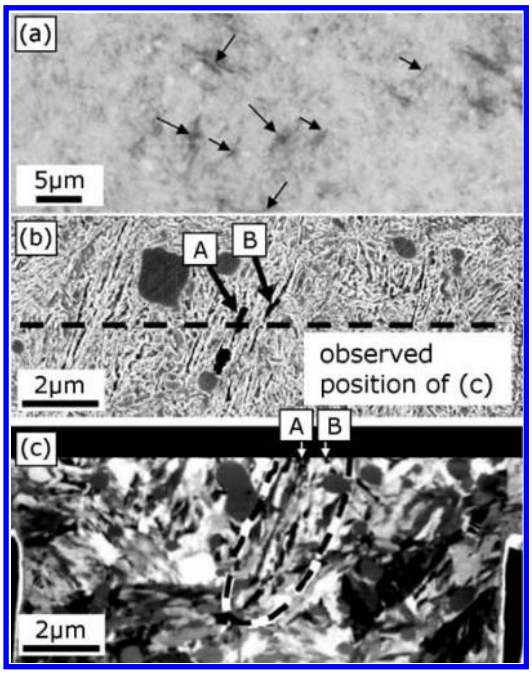

16 Microstructural changes in roller on disc specimens. *a* Optical image, black arrows show acicular structures. *b* Scanning ion microscopy (SIM) image of black acicular structure in plane of OM image in *a*. *c* SIM image of cross-section of dotted line in *b*, the dotted line surrounds microstructure which seems to have changed, which was confirmed by TEM/selected area diffraction patterns (SADP). Cycles=$4{\cdot}7\times10^6$, max. contact pressure=4·2 GPa, speed=3000 min^{-1}, slip ratio of 14% applied by spin. Adapted from Ref. 30

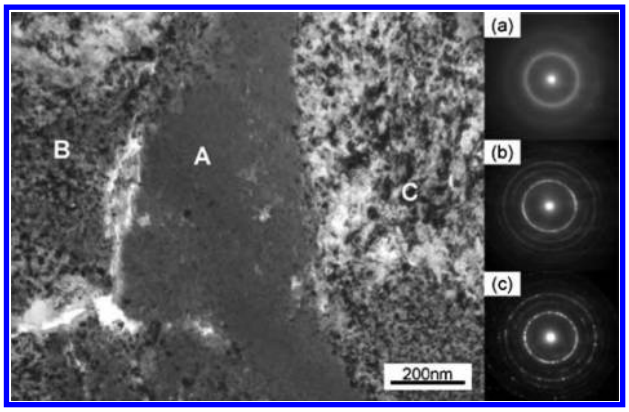

17 Bright field image (TEM) and selected area diffraction patterns (SADP) of WEA. Selected area diffraction patterns of microstructural areas A, B and C are shown in photos *a*, *b* and *c* respectively. B and C contain granular structures whereas A is absent of these. Selected area diffraction pattern of *a* corresponds to A showing halo rings, thus indicating an amorphous structure, whereas *b* and *c* are a mixture of ring and spot patterns consistent with ferrite and nanograin structure[30]

large grain boundary area.[26,47,114] Dislocation density of WEA in butterfly wings is estimated as about 10^{16}–10^{17} m^{-2};[29] however, a high dislocation density is not observed within nanoferrite grains themselves[45] due to their small size; thus, it is suggested that dislocations are mostly accommodated at grain boundaries (dislocation networks)[45] where enrichment of carbon at grain boundaries will occur as dislocations migrate from grain interiors to grain boundaries, dragging along carbon atoms. However, as a high carbon concentration is detected within nanograins, a certain level will be interstitially dissolved in the ferrite. It is suggested that carbon will also be accommodated by migration to WEA borders to precipitate as lenticular carbides which is consistent with pressure raising the activity level of carbon, where lenticular carbides have been observed bordering WEA.[25,45,47] Carbide precipitation at grain boundaries may result in intergranular crack generation.[45] Tempering of steel containing WEA has shown to reprecipitate carbides, which is expected by reduction in dislocation density and removal of stress in WEA.[47] The WEA typically has hardness 30–50% higher than the matrix,[23,27,40] this difference being removed by subsequent heating to 500°C in AISI 52100 steel.

Owing to the cyclic stress, spherical carbides within the WEA appear elongated and deformed at early stage, finally resulting in break-up and dissolution,[21,30,40,42,46,47] with shear flow of carbides towards the crack (Fig. 15)[115] and interface between WEA and the inclusion.[18,25,28,29,45] Diffusion of carbon interstitially bonded to carbide into the microcrack will reduce its surface energy and be favourable for its stable growth.[25]

Harada *et al.*[30] proposed that black acicular structures, having a structure in which martensite laths are broken down and changed to granular structure, are the initial process of WEA formation (Fig. 16). These form at angles of 30 and 160° to the rolling direction, indicating directions of shear stress from slip in the contact. The WEA is differentiated by amorphous-like regions[29,30] (Fig. 17) containing the smallest grains, and areas in between amorphous regions containing larger

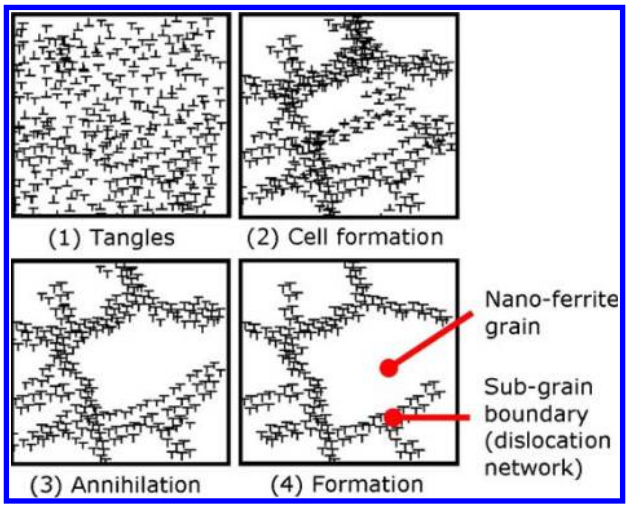

18 Polygonisation: generation of subgrains by clustering of dislocations in networks. Adapted from Ref. 116

grains. Microcracking is also present at the interface of amorphous/granular phase and WEA/matrix, and microvoids are formed at the interface of retained austenite/martensite and spheroidised carbide/martensite.[30] It is supposed that the amorphous-like structures form first, then WEA is generated.

The WEA has been suggested to form by the hydrostatic pressure forcing crack surfaces to close causing nanocrystallisation.[28] Finite element stress analysis has shown that WEA is generated in a specific microcrack kink region where hydrostatic compressive stress is locally high.[28] Microcracks were thought to be prerequisites to WEA formation, where hydrostatic pressure is thought to suppress microcracks and therefore assist in accumulation of plastic strain and thus WEA formation.[39] Because of the lower density of carbide compared with ferrite, hydrostatic pressures would cause solution of the carbide.[47] Nanocrystallisation of butterfly wings may be driven by large plastic strains developed ahead of the crack tip extending from the inclusion, which would suggest that cracks form first, then WEA is subsequently formed. Other earlier investigations supposed that crack closure results in heating to austenitising temperature, self-quenching and rehardened martensite forming.[18,113] Other investigations supposed that severe deformation of the carbides is what causes their dissolution, rather than heating to high temperatures,[80] which is not thought to occur in operation. Polygonisation has also been suggested for WEA formation[45] (Fig. 18)[116] and also for formation of 'fine granular area' around inclusions in rotating bending testing of high chromium bearing steels.[117]

Owing to local stress concentration at hard inclusions, it was proposed that dislocation generation and movement (glide) from the interface of the inclusion/matrix occurs,[107] where WEA formation is due to the repeated interaction of dislocations with carbide precipitates causing carbide break-up and dissolution. However, it has been contested that dislocations sweeping the entire butterfly wing are correct, as in hard steels, there are many obstacles (carbide precipitates, high density of dislocations, vacancy clusters, etc.) strongly limiting average dislocation glide during each stress cycle.[26]

Harada *et al.*[30] proposed that acicular structures and WEA formation occur from localised shear in martensite and localised plastic strain causing increased dislocation density, and when a critical dislocation density is reached, a dislocation cell-like structure forms to release the strain energy. Dynamic recrystallisation is proposed to change this cell-like structure to minute grain structure.[118] However, supposedly dynamic recrystallisation is not valid in RCF bearing steels due to a lack of time in the stress cycle and thermal activation, instead a low temperature recrystallisation process is postulated,[26] taking place over a longer time period in between stress events.[29] The theory states that as plastic deformation results in a high density of dislocations and crystal point defects (the later stabilised by carbon in the solid solutions),[119] there is now no need to thermally activate the formation of vacancies, their mobility being invoked during normal operation. Referring to Fig. 14*d*, the grain refinement and smaller KAM inside WEA close to the inclusion are postulated to be caused by plastic deformation and immediate incomplete recrystallisation, which leads to a clean of dislocation volume in the grains, but high misorientation still remaining next to the grain boundaries.[23]

Referring to white phase in other applications, WELs on rail steel surfaces and hard turning consist of a nanograined structure with associated carbide dissolution, supposedly supersaturated with carbon, where in WEL in hard turning, plastic deformation or thermal transformation is cited[8,9] and on rail tracks, high temperatures by sliding and cyclic plastic deformation is cited.[14,120] However, in rail steels, reaustenitisation temperatures of 600°C do not occur[14] where surface temperatures rapidly decrease subsurface.[13] The decomposition of carbides and formation of nanocrystalline structures also occur in high pressure torsion,[120] ball drop and laser heating,[121] ball milling[122,123] and heavily drawn pearlitic steels.[114,124–126] In all these applications, the mechanisms for nanograined structures, carbon dissolution and carbon distribution are not fully understood.[127] Often techniques such as Mössbauer spectrography, synchrotron X-ray diffraction and atom probe tomography are used in these applications to understand carbide dissolution and carbon distribution, and could be possibly applied to WEA in rolling contacts to gain a better understanding of WEA formation mechanisms and material solutions.

Butterfly and WEC formation thresholds

Contact pressures used to create butterflies and WEC in laboratory very generally range between 1·4 and 5·5 GPa with rolling cycles of 10^5–10^8. Wind turbine gearbox bearing raceways would typically experience a contact pressure of 1–2 GPa during normal operation; however, transients in service could result in much higher stresses intermittently, perhaps providing critical stresses in excess of thresholds to continue crack propagation from butterflies into the matrix for example. However, maximum contact pressure and number of rolling cycles are not the only driving variables in WSF, as highlighted in the next section.

White structure flaking formation drivers

Influence of hydrogen

Hydrogen is often cited as a root cause or accelerator of WSF,[3,4,30,32–39,43,44,50–57] though not always.[5,42,58] Hydrogen in its natural state is diatomic molecular gas, H_2, this being

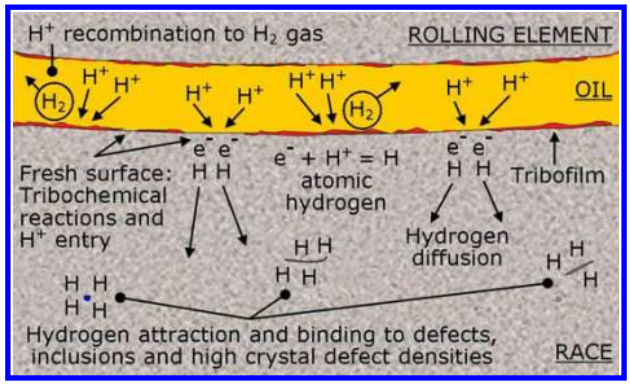

19 Schematic of rolling element and race lubricated with oil, or similarly grease, containing hydrogen radicals. Hydrogen ions (H^+) combine with electrons (e^-) at fresh steel surfaces to form atomic hydrogen (H). Recombination of H^+ to H_2 gas can be inhibited by poisoners such as sulphur, leading to more hydrogen ions and thus atomic hydrogen in the steel. Atomic hydrogen attracts and strongly binds to crystal defects. Copyright M.-H. Evans

too large to enter steel, and must therefore be dissociated into single atoms to enter the surface, electrochemically or by chemisorption.[128] Sources of hydrogen are dissociation from water,[85,129,130] degradation of organic lubricants through formation of compounds (hydrogen peroxide),[129] oxidation,[4,44,85] pressure/thermally induced,[43] and contained in steel from heat treatment processes. However, through hardened steel is tempered, so high concentrations of hydrogen are not expected (tempering releases trapped hydrogen); also there is no effect on WSF life between normal and vacuum quenched steels (i.e. no hydrogen entry upon quenching).[4] A catalytic reaction with a fresh steel surface, and not shear or heat, has been found to dominant in hydrogen disassociation from lubricants, and the amount of hydrogen which penetrates into steel is proportional to the wear on the steel, rather than any effect of lubricant chemical composition.[52] Hydrogen ions released are absorbed by fresh steel surfaces and recombine with electrons to form atomic hydrogen[57] (Fig. 19). When water is present, hydrogen mainly derives from the oil and not water.[131]

Hydrogen precharging samples[4,33,38,39,43,44,85,106,130–134] or testing in hydrogen gas environments[32,34,37,85] have been used to study hydrogen influence on fatigue life by RCF, tensile,[106,130] tension–compression,[132,135,136] pure, sliding and rolling rotating bending,[130] and cyclic torsion[134] experiments. In the later, slip bands and microstructural changes only occurred in specimens charged with hydrogen. In general, a decrease in fatigue life and strength occurs with hydrogen charging where in RCF bearings fail from WSF. Damage to the passivation layer (oxide layer formed from oxidisation) on steel by wear or corrosion provides a fresh steel surface which accelerates hydrogen absorption. Hydrogen penetration into steel during RCF tests has also been observed,[3,4,36,37,43,44,51–53,85,137] for example up to 4·2 ppm,[43] often with the zones of test samples with the highest content of hydrogen failing first, with critical average concentrations of hydrogen cited, e.g. 1 ppm.[43] Average hydrogen contents tend to be measured by thermal desorption analysis using mass spectroscopy and gas chromatograph analysers; however, local concentration can be high compared with average levels due to redistribution within the matrix,[130] also some hydrogen will remain trapped in the steel, e.g. at voids.[85] Samples are often frozen immediately after testing with dry ice or liquid nitrogen to stop hydrogen escaping.[38,39,43] Other research has estimated hydrogen content in the surface layer of AISI 52100 steel balls to be 24 ppm[85] and higher in specific regions near the surface.

Environmental fluctuation (i.e. cyclic charging) rather than hydrogen content may affect susceptibility to hydrogen.[138] Trapping and diffusion of hydrogen becomes more intense with increased external stress[106,130] and stress cycles,[130] and plastic or thermal deformation of surfaces makes hydrogen diffusion easier.[85,139] Hydrogen diffusivity (speed) and not flux (quantity) may be the critical parameter in WSF.[3,4]

Atomic hydrogen is attracted to and absorbed at grain boundaries, carbides, inclusions, microvoids, isolated islands of phases such as austenite and areas of local plastic deformation where crystal defect densities (dislocations/vacancies) are high because hydrogen strongly binds with crystal defects.[85,106,140–146] Hydrogen trap sites within steel can be reversible or non-reversible, attractive or repellent. As an interstitial solute, hydrogen remains in the monoatomic form and retains its mobility in high strength steels,[132] being only loosely bound to weak traps, such as dislocations and point defects[138,146–148] but also to a small degree as vacancy–hydrogen pairs.[33] The WEC forming at former austenite grain boundaries (unstable trap sites and diffusion routes) has been found.[3,43] High chromium steels, having strong hydrogen trapping functions, retard hydrogen diffusion and thus hydrogen

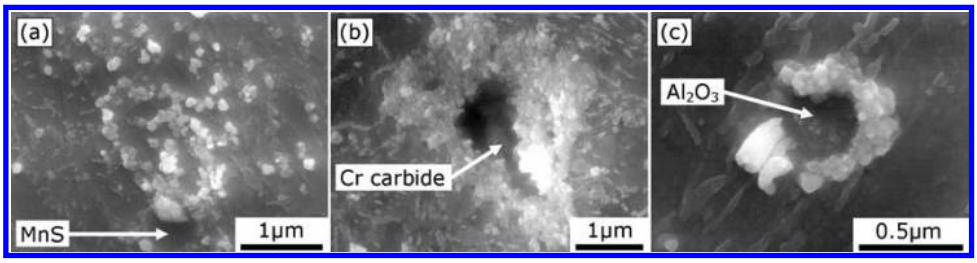

20 Field electron SEM image of the autoradiograph around MnS and Al_2O_3 inclusions and Cr carbide in JIS-SCM440 tempered martensitic steel (0·4 wt-%C, 0·21 wt-%Si, 0·79 wt-%Mn, 1·2 wt-%Cr and 0·21 wt-%Mo). Bright white spots are Ag grains (hydrogen atoms) corresponding to locations of tritium. *a* MnS: Ag grains appear on cementite particles precipitated in high angle boundaries such as block, packet and prior austenite grain boundaries but not in the matrix, indicating cementite particles acting as traps around the inclusion. *b* Cr carbide: Ag grains accumulated at the boundary layers between Cr carbide and matrix. *c* Al_2O_3: Ag grains accumulated at the boundary layers of the matrix surrounding the inclusion with no widely distributed Ag grains. Adapted from Ref. 149

cannot accumulate easily.[51,85] Decreasing large MnS inclusions, which are weak hydrogen traps that release hydrogen into a high shearing stress field, improves WSF life,[57] on the other hand, a limited number of non-reversible traps may increase propensity to WSF.[141] This appears to be a contradiction; however, it may be that as steels get cleaner, there are less trapping locations for any possible hydrogen present in the steel, thus instead of hydrogen trapping at less critical defects, instead the hydrogen remains mobile and moves to more critical defects and locations of plastic deformation, accelerating white structure formation.

Autoradiography showed hydrogen trapping to predominately occur at martensite matrix/carbide and carbide/carbide interfaces in AISI 440C steel,[106] and vary depending on the type of inclusion.[145] Hydrogen was inhomogeneously distributed at defects around the matrix surrounding MnS (Fig. 20*a*),[149] at boundary layers between the Cr carbide and matrix (Fig. 20*b*), but intensely localised at defects in the boundary layers surrounding Al_2O_3 (Fig. 20*c*), which was attributed to the differing CTE when cooled during quenching, and thus compressive stress fields around MnS and tensile around Al_2O_3 and Cr carbide.

The hydrogen enhanced decohesion[150] model is based on the theory of weakening of the lattice strength by hydrogen. The hydrogen enhanced localised plasticity[151] model is based on *in situ* TEM observation of dislocation movement which has been enhanced by hydrogen. Both theories are lacking, in that direct observation of lattice decohesion in hydrogen enhanced decohesion has not been observed and fracture phenomenon caused by hydrogen enhanced localised plasticity has not been observed,[136] and neither are individually able to explain hydrogen embrittlement on the nanoscale.[152] Hence, hydrogen reducing the required stress for the onset of plasticity,[132,140,153–155] i.e. dislocation nucleation increasing the number and mobility of vacancies (mobile crystal point defects)[132,133,138,140,142,146,148,152] is suggested to occur by reduction in the shear modulus (by reduction in crystal cohesion) and reductions in dislocation line energy and stacking fault energy (by reduction in the defect formation energy).[152] Hydrogen enhances slip deformation and localised slip bands, accelerating modes I and II crack growth rates,[134] and reduces the strength of hard martensite matrix.[135] It is suggested that hydrogen enhances fatigue crack initiation and propagation by localisation of plasticity at fatigue crack tip.[134,136] Vegter and Slycke[33] explain that with hydrogen's formation enhancement of vacancies, this enhances the dislocation climb controlled damage process,[134] which with hydrogen's attraction to point defects, results in a self-generating damage localisation process and lowering of WEA formation thresholds.

Clearly, if hydrogen diffusion occurs in steel, it is detrimental; however, further study into the propensity of hydrogen diffusion into wind turbine gearbox bearings is required to understand if high levels of hydrogen do indeed occur in service, or whether other potential formation drivers require more attention.

Tribochemistry, lubrication and additives

Lubricants can be in the form of grease or oil, where wind turbine gearboxes mainly use oils with high viscosity (ISO-VG 220-320), at operating temperatures of 60–85°C.

Often wind turbine gearbox bearings run in mixed and boundary lubrication regimes rather than elastohydrodynamic lubrication, where this can result in high traction coefficients resulting in shearing of the steel and metal–metal contact, with peak contact pressures and temperature flashes occurring at asperities. Under rolling/sliding, tribofilms form at contact surfaces with various morphologies and thicknesses depending on the lubrication and steel type (Fig. 4), with tribomutation layers forming subsurface.[83,156] Reaction flash temperatures at asperities dominate in formation of tribofilms rather than nascent surfaces.[157] Tribofilms provide significant adhesion protection under severe plastic deformation and lubricant starvation,[156] and provide a barrier to corrosion and hydrogen diffusion into steel if continuous and intact.

Extreme pressure (EP) additives typically consist of sulphur, phosphorous or chlorine compounds, chemically reacting at the surface under extreme pressure and temperature flashes. Tests on AISI 52100 showed phosphorus enhanced films forming first on fresh surfaces, then sulphur enhanced films forming under increased loads and temperatures to prevent metal–metal contact.[158] However, chemically active EP additives, e.g. sulphur–phosphorous, can be detrimental to RCF life,[159] accelerating the progress of surface fatigue microcrack propagation when inside fissures in contact with a fresh steel surface,[160] and antiwear additives can produce an increase in friction and reduction in oil film thickness.[161] Sulphur prevents atomic hydrogen recombination to H_2 gas, thus enabling more hydrogen ions to combine to form atomic hydrogen[162] (Fig. 19). Most lubricant compositions comprise of a rust preventative such as sulphonates which can increase WSF propensity,[44,54,55] where rust preventatives keeping surfaces clean accelerate WSF, whereas rust preventatives deactivating surfaces prevent WSF.[44] Additives such as oxidised iron powder,[44] copper powder[44] and aluminium oxide[54] accelerate WSF. Foaming of lubricants occurs in wind turbine gearboxes due to entrained air, where bubble collapse could cause surface damage.

With regard to tribological preventative measures against WSF, during WSF rapid acceleration–deceleration and impact loading tests on greases in automotive bearings, grease with extended life showed wider and shallower load zones, resistance to impact load film breakdown, lower repulsion coefficient, lower maximum vibration level close to resonance (by a factor of 2), and the grease containing an adhesive substance, all these increasing damping characteristics and hence reduction in peak and impact loads.[42] Fluorine based oils (e.g. PFPE) and fluorine based surface active agents (forming raceway films) have been suggested as partial preventers of water ingress and WSF,[52,55] containing no hydrogen radicals and thus not producing hydrogen;[52] however, perhaps WSF still occurs with their use[58] showing that hydrogen decomposition (from lubricants) is not necessary for WSF to occur. Isopropylaminoethanol additive condenses into surface microcracks with water, capturing generated hydrogen ions and thus preventing hydrogen enhanced crack propagation[163] and hence possibly WSF. Lubrication with increased heating stability, specifically synthetic ether[44] and Al metal powder increases WSF life.[54] $NaNO_2$ and K_2MoO_4 anodic corrosion inhibitors (which reduce anode reactions by oxidising steel, with

adsorption and reaction of oxidising ions or dissolved oxygen) forming a metal oxide film,[32,52,54] $ZnCO_3$ cathodic corrosion inhibitor (which decreases cathode reactions by formation of anticorrosion films) and rust preventatives/metal deactivators naphthenate (e.g. Zn),[55] succinic acid derivative (metal DTC or DTP)[55] and organic metal salts (preferably Zn based)[55] which form a reactive film in a minute gap, prevent hydrogen penetration or WSF in tests. However, merely reducing fresh steel surfaces by reducing wear by antiwear additives does not reduce hydrogen penetration into steel[52] and phosphate additives forming a film which has a high antiwear property to suppress generation of hydrogen are ineffective,[32,54] because of a lack of thermal activation to form a film.[32]

Clearly, damage exposing fresh steel surfaces is detrimental to bearings in itself, acting as a catalyst for tribochemical reactions or corrosion. Hence, a greater understanding of tribofilm formation and oil additive packages which are designed specifically for use with both gears and bearings in wind turbine gearboxes is required to prevent WSF.

Water

White structure flaking has been reproduced by adding water to the lubricant[4] either causing corrosion which enhances hydrogen diffusion into steel, formation of atomic hydrogen by creation of hydrogen peroxide[129] or formation of fresh surfaces leading to hydrogen generation. A major contaminant in wind turbine gearboxes is water ingress[1] sourced from coolants and condensation[50] (as wind turbines slow down to standstill, they cool down and draw moisture from the air, i.e. as the gearbox breathes through seals and breathers, water can enter the gearbox), or *in situ* from the oxidative decomposition of oil.[85] Water attracts to surface microcracks, liberating hydrogen at fresh surfaces inside the crack.[160] Water transforms sulphur phosphorous EP additives into acids, resulting in a corrosive acidic fluid environment.[1,160] Small water globules pulled in between contacting surfaces result in collapsed oil film strength and lost clearance, causing impacts and rubbing of opposing contact surfaces.[1,160]

Contact slip and traction

There are two ways that slip could be a driver of WSF, first directly by creation of surface traction and shear stresses shifted closer to the surface and their damage influence.[3,30] For example, slip can result in high frictional energy input which rapidly accelerates surface fatigue and high traction coefficients thus shearing the material, shifting the position of subsurface shear stresses closer to the surface and increasing their magnitude[80,164] which would increase probability of WSF from inclusions and thus butterflies which form in the very near surface zone. Second, indirectly by tribofilm damage and creation of fresh surfaces liberating hydrogen.[52]

Slip is inevitable in bearings and occurs in operation at loads below the dynamic load rating, at misaligned rollers in unloaded zones due to low traction forces, as 'heathcoat slip' in spherical roller bearings due to a geometrical constraint[1] and during transient events in transmissions, such as rapid accelerations–decelerations.[165] Simulations have shown that for cylindrical roller bearings in an intermediate shaft location of a wind turbine gearbox, moderate sliding (3–10% slide to roll ratio) at roller–raceway contacts in the unloaded zone occurs continuously.[165] Extreme slip (about 20–110% slide to roll ratio) occurs for low load and high speed conditions due to concomitant contact area reduction and traction loss at roller/raceway interfaces.[165]

Slip to varying degrees is often used in rolling contact studies;[3,4,30,36,42,44,49,54,55,57,83,166] often this being quoted essential in creating white structures. It was found that WSF only occurs at specific regions having the largest PV_{max} value (a product of contact pressure P and slip velocity V, MPa m s^{-1}) in bearings due to these regions corresponding to the highest concentrations of hydrogen.[3,36] Slip can also shear and heat the lubricant, reducing oil film thickness[167,168] which may lead to wear and hydrogen liberation. However, a high slip ratio does not necessarily mean that shearing of contacting surfaces is high, and it is the traction coefficient that limits the amount of shear induced in the contacting materials, and thus this, lubricant regime and frictional energy input should be the key parameters in tribological experiments if aiming to replicate actual service operating conditions or perhaps aiming to create WSF.

Corrosion and standstill time

Water, sea water and salt contamination from offshore environments are possible in wind turbine gearboxes, where these can often experience long standstills and idling operation. Thus corrosion, static corrosion and fretting corrosion (movement between the element and race by vibration for example, resulting in passivation films being removed and nascent steel surfaces being exposed to corrosion from the atmosphere) are possible. Corrosion as a mechanism of hydrogen liberation may be an indirect driver, but also hydrogen enhanced diffusion to the subsurface at corrosion damage on the raceway surface and corrosion within microcracks generated from operation.[163]

Electricity

Lightning strikes and stray currents could affect bearings in wind turbine gearboxes. Electricity may cause WSF indirectly, through wear or arcing damage by current on bearing surfaces, which produce fresh steel forming hydrogen,[54] or by liberation of hydrogen by electrolysis. Studies show that the larger the current (0·1–3 A), the earlier the occurrence of WSF,[54] where more wear occurs on the ring at the electrically positive pole thereby corresponding to the location of WSF. Static electricity (several hundred thousand volts) has been cited to indirectly cause WSF in automotive bearings, by building up between contacting surfaces (due to a belt driving the assembly) and subsequently discharging (spark) when metal–metal contact occurs (from oil film deterioration by static electricity during periods of excessive microslip or vibration) which liberates hydrogen from water in the lubricant.[4] Use of hybrid bearings (ceramic elements) and conductive lubrication (carbon black/nanotube additives) which prevents a static electricity discharge phenomenon between contacting surfaces liberating hydrogen from water in the lubricant, has been shown to prevent this phenomenon.[4]

Impact loading

Impact events are frequently experienced in wind turbine gearboxes, by wind gusts, braking, load reversals and generator/grid engagements and disengagements. In the unloaded zones of rolling element bearings, repeated

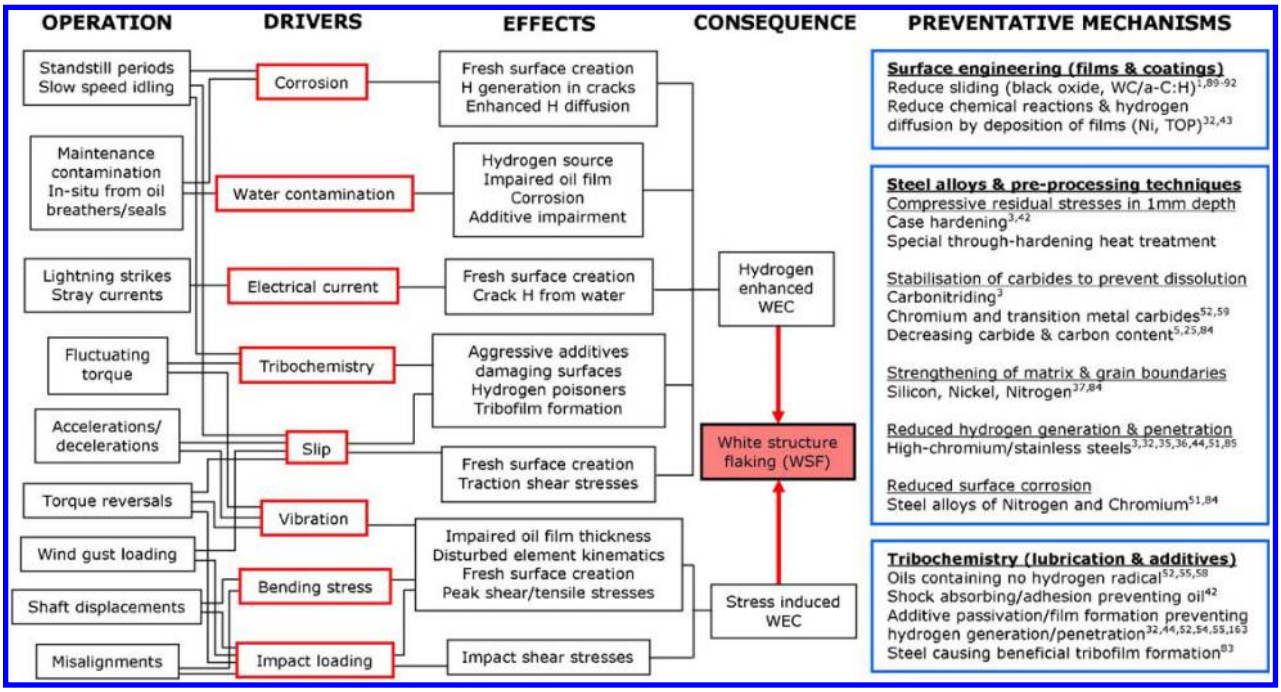

21 White structure flaking formation driver summary in wind turbine gearboxes and possible solutions. H=hydrogen. Copyright M.-H. Evans

impacts occur when elements are instantaneously loaded while in misaligned conditions along one or two contact points in the load profile.[60] Therefore, contact stresses exceeding yield strength can be experienced. For example, a 600 mm displacement of an intermediate shaft from a 1·5 MW gearbox resulting in severe misalignment[60] can produce a predicted transient raceway stress exceeding 3·1 GPa.[1] The WEC in automotive belt driven bearings may be caused by collisions of rolling elements,[58] where during rapid acceleration–deceleration, impact loads in 0·3 s have been found to occur, which were attributed to the reduction in WSF life.[42] Even though predicted loading in wind turbine gearbox bearings is a maximum of ~2 GPa, condition monitoring of loading in actual gearbox bearings may not have a high enough sampling rate to register instantaneous impact loads.

Vibration, bending stress and tensile hoop stress

Bending stress, tensile hoop stress and vibration theory as mechanisms increasing maximum loads have been cited,[42] where severe vibrations have been induced to create WSF[3,4,42,44,49,54,58] and resonance applied on a belt driving a bearing.[42,58] Vibrations in wind turbines can occur from blades and blade revolution frequency, from grid connections, brake loads and nacelle deflections. Vibrations may influence oil film formation leading to formation of fresh surfaces, increase peak loading, or disturb the kinematics of the rolling elements.

Conclusion and further research

Figure 21 shows a schematic diagram of formation drivers, where many stimuli to the system have a possible consequence of hydrogen theory.

1. A greater understanding of transient loading and tribological conditions faced on wind turbine gearbox bearings is required, such as the high likelihood that large impact loads occur in service, which would enable bearing and gearbox designers to devise material and design solutions for known operating conditions.
2. Cyclic subsurface shear stresses induced in over-rolling often do not fully explain the location and orientation of white structures, thus a greater understanding of the cyclic multiaxial stress state potentially driving white structure formation is required.
3. Non-metallic inclusions and defects initiate butterflies, where inclusion size, morphology, orientation in the stress field and composition determine severity.
4. The WEC probably initiates subsurface, possibly from extension of butterfly cracks, but surface initiated is also feasible, where this should be clarified by a method for mapping the three-dimensional WEC system. As a sequence of events, either butterflies form first at an early stage, some propagating to initiate WEC, or butterflies and WEC form independently, where in both cases WEC propagates to result in WSF.
5. High traction coefficients raise subsurface shear stress location close to the surface and increases its magnitude, perhaps making it more likely for butterfly propagated WSF in this zone from near surface inclusions.
6. It is not known whether cracking or white structure occurs first, where cooperative growth is also cited, or whether white structure is integral to WEC formations, formed for example by frictional rubbing between crack faces or a consequence of significant accumulation of plastic strain.
7. Formation mechanisms of white structure that consists of ultrafine ferrite grains of 10–100 nm diameter that is supersaturated with carbon, by dislocation, carbon, carbide influence and recrystallisation are contested.
8. WEC drivers
   (i) Stress:
   Vibrations, peak loads, slip, traction, bending and tensile hoop stress.
   (ii) Hydrogen influence:
   Hydrogen release, poisoners and tribofilm effects:
   • Oil and additive systems

Hydrogen source fresh surface creation:
- Water contamination

Hydrogen disassociation and fresh surface creation:
- Slip, traction, corrosion and electrical discharge

Fresh surface creation:
- Impact loads and vibration

9. Hydrogen can be present in bearing steels from various sources, such as water contamination and disassociation from lubricants. It is clear that hydrogen within the microstructure lowers thresholds for crack initiation and propagation; however, the mechanism of hydrogen as a root cause of WSF needs to be clarified. Many formation drivers also indirectly aid hydrogen generation and diffusion, making verification of other drivers difficult. Bearing hydrogen content could be measured soon after operation, incorporating a freezing process, to deduce any possible acceleration of damage.

10. Lubrication and additive selection can significantly accelerate or retard WSF, which is usually explained by deleterious effects from hydrogen influence. Additives either accelerate or decelerate corrosion, wear, electrical effects, tribochemical reactions and hydrogen generation/diffusion and can prevent surface damage from sliding, adhesion, vibration and shock loads.

11. Steels containing reduced quantity of carbon and size of carbides in the $\sim$1 mm surface layer, case hardened steels such as carbonitrided steels, high chromium steels and low carbon stainless nitrogen alloy steels show improved WSF life. Elements which strengthen the matrix and grain boundaries and beneficial compressive stresses may also prevent or prolong WSF. The inhibition of hydrogen influence by reduced wear, enhanced corrosion resistance, matrix strengthening and carbide stabilisation is cited; however, the mechanisms for improved performance are not fully understood and solutions may be unacceptably expensive.

12. Surface engineering by formation of protective films or surface coatings on contacting surfaces which diffuse into the steel raceway, reducing hydrogen generation/diffusion and friction from slip can improve WSF life, though often their preventative mechanisms and long term effects on components are unknown.

13. Few systematic studies have been conducted with the aim of identifying tribological formation drivers in WSF, thus making it difficult to identify WSF drivers. Extensive testing in laboratory is required to understand mechanisms behind drivers and solutions to help prolong lives of wind turbine gearbox bearings.

14. It is clear from this review that the WSF theories presented are complex and ideas often speculative. There is much further work to be conducted to prevent these failures, especially as the size of wind turbines is rapidly increasing, resulting in more extreme operating conditions and the quality of steel for larger bearings becoming more critical. An interesting question is why this failure has only seemingly surfaced extensively in the last one or two decades and why it is not more widely known in other industries apart from automotive and wind.

Acknowledgements

The support and informative discussions with sponsors, Dr C. Højerslev, Mr M. Lewis, Mr G. Plint, Dr B. G. Mellor, Professor R. Wood and Dr L. Wang are greatly appreciated, as it the FIB work conducted by Dr J. C. Walker at the Southampton Nano-Fabrication Centre (SNC).

References

1. M. N. Kotzalas and G. L. Doll: 'Tribological advancements for reliable wind turbine performance', *Phil. Trans. R. Soc. A*, 2010, **368A**, (1929), 4829–4850.
2. K. Ihata, T. Shiga and A. Umeda: 'Rolling bearing assembly having magnet to prevent brittle flaking', US Patent 7,520,675 B2, 2009.
3. S. Tanaka, N. Mitamura and Y. Murakami: 'Influence of sliding and chromium content in the steel on the white structural change under rolling contact', Proc. Global Powertrain Cong., Dearborn, MI, USA, September 2004, Global Powertrain Congress, Vol. 32, 6–13.
4. K. Iso, A. Yokouchi and H. Takemura: 'Research work for clarifying the mechanism of white structure flaking and extending the life of bearings', SAE World Cong., Detroit, MI, USA, April 2005, SAE International, Paper 2005-01-1868.
5. J. Luyckx, W. Broeders and J. Geertsom: 'Method for increasing the fatigue strength of a predominantly steel mechanical part of a wind turbine and/or for reducing the tendency to form what are called 'white etching cracks' or 'brittle flakes' in such steel mechanical parts', US Patent 2009/0288742 A1, 2009.
6. Northwest Laboratories of Seattle, Inc., Seattle, WA, USA, 2007.
7. Wind turbine gearbox reconstruction in Fig. 3 based on model from National Renewable Energy Laboratory (NREL), Gearbox Reliability Collaborative.
8. J. Barry and G. Byrne: 'TEM study on the surface white layer in two turned hardened steels', *Metall. Mater. Trans. A*, 2002, **325A**, 356–364.
9. A. Ramesh, S. Melkote, L. Allard, L. Riester and T. Watkins: 'Analysis of white layers formed in hard turning of AISI 52100 steel', *Mater. Sci. Eng. A*, 2005, **A390**, (1–2), 88–97.
10. D. Schwach and Y. Guo: 'A fundamental study on the impact of surface integrity by hard turning on rolling contact fatigue', *Int. J. Fatigue*, 2006, **28**, (12), 1838–1844.
11. G. Baumann, K. Knothe and H.-J. Fecht: 'Surface modification, corrugation and nanostructure formation of high speed railway tracks', *Nanostruct. Mater.*, 1997, **9**, 751–754.
12. R. Carroll and J. Beynon: 'Rolling contact fatigue of white etching layer: Part 1 crack morphology', *Wear*, 2007, **262**, (9–10), 1253–1266.
13. I. M. Widiyarta, F. J. Franklin and A. Kapoor: 'Modelling thermal effects in ratcheting-led wear and rolling contact fatigue', *Wear*, 2008, **265**, (9–10), 1325–1331.
14. G. Baumann, H. J. Fecht and S. Liebelt: 'Formation of white-etching layers on rail treads', *Wear*, 1996, **191**, 133–140.
15. H. Yokoyama, S. Mitao, S. Yamamoto, Y. Kataoka and T. Sugiyama: 'High strength bainitic steel rails for heavy haul railways with superior damage resistance', *NKK Tech. Rev.*, 2001, **84**, 44–51.
16. T. W. Wright: 'The physics and mathematic of adiabatic shear bands'; 2002, Cambridge, Cambridge University Press.
17. S. M. Walley: 'Shear localization: a historical overview', *Metall. Mater. Trans. A*, 2007, **38A**, (11), 2629–2654.
18. H. Schlicht, E. Schreiber and O. Zwirlein: 'Effects of material properties on bearing steel fatigue strength', in 'Effect of steel manufacturing processes on the quality of bearing steels', (ed. J. J. C. Hoo), 81–101; 1988, Philadelphia, PA, ASTM.
19. A. P. Voskamp, R. Österlund, P. C. Becker and O. Vingsbo: 'Gradual changes in residual stress and microstructure during contact fatigue in ball bearings', *Met. Technol.*, 1980, 14–21.
20. I. A. Polonsky and L. M. Keer: 'On white etching band formation in rolling bearings', *J. Mech. Phys. Solids*, 1995, **43**, 637–669.
21. H. Swahn, P. C. Becker and O. Vingsbo: 'Martensite decay during rolling contact fatigue in ball bearings', *Metall. Trans. A*, 1976, **7A**, 1099–1110.
22. T. A. Harris and M. N. Kotzalas: 'Rolling bearing analysis – essential concepts of bearing technology'; 2007, Boca Raton, FL, Taylor & Francis.
23. A. Grabulov, R. Petrov and H. W. Zandbergen: 'EBSD investigation of the crack initiation and TEM/FIB analyses of the microstructural changes around the cracks formed under rolling contact fatigue (RCF)', *Int. J. Fatigue*, 2010, **32**, (3), 576–583.

24. T. B. Lund: 'Subsurface initiated rolling contact fatigue – influence of non-metallic inclusions, processing conditions, and operating conditions', *J. ASTM Int.*, 2010, **7**, (5), 1–12.
25. K. Sugino, K. Miyamoto, M. Nagumo and K. Aoki: 'Structural alterations of bearing steels under rolling contact fatigue', *ISIJ Int.*, 1970, **10**, 98–111.
26. A. Grabulov: 'Fundamentals of rolling contact fatigue', PhD thesis, University of Belgrade, Serbia, 2010.
27. P. C. Becker: 'Microstructural changes around non-metallic inclusions caused by rolling contact fatigue of ball-bearing steels', *Met. Technol.*, 1981, **8**, 234–243.
28. K. Hiraoka, M. Nagao and T. Isomoto: 'Study on flaking process in bearings by white etching area generation', *J. ASTM Int.*, 2006, **3**, (5), 1–7.
29. A. Grabulov, U. Ziese and H. W. Zandbergen: 'TEM/SEM investigation of microstructural changes within the white etching area under rolling contact fatigue and 3-D crack reconstruction by focused ion beam', *Scr. Mater.*, 2007, **57**, (7), 635–638.
30. H. Harada, T. Mikami, M. Shibata, D. Sokai, A. Yamamoto and H. Tsubakino: 'Microstructural changes and crack initiation with white etching area formation under rolling/sliding contact in bearing steel', *ISIJ Int.*, 2005, **45**, (12), 1897–1902.
31. D. Scott, B. Loy and G. H. Mills: 'Metallurgical aspects of rolling contact fatigue', *P. I. Mech. Eng.*, 1966, **181**, (315), 94–103.
32. T. Endo, D. Dong, Y. Imai and Y. Yamamoto: 'Study on rolling contact fatigue in hydrogen atmosphere – improvement of rolling contact fatigue life by formation of surface film', Proc. 31st Leeds-Lyon Tribology Symp.: 'Life cycle tribology', (ed. D. Dowson *et al.*), 343–350; 2004, Leeds, Elsevier.
33. R. H. Vegter and J. T. Slycke: 'The role of hydrogen on rolling contact fatigue response of rolling element bearings', *J. ASTM Int.*, 2009, **7**, (2), 1–12.
34. Y. Imai, T. Endo, D. Dong and Y. Yamamoto: 'Study on rolling contact fatigue in hydrogen environment at a contact pressure below basic static load capacity', *Tribol. T.*, 2010, **53**, (5), 764–770.
35. X. D. Peng, Y. Shimizu and N. Mitamura: 'Long life bearing technologies on material aspect', in 'Advanced tribology', (ed. J. Luo *et al.*), 932–933; 2010, Berlin, Heidelberg, Springer.
36. S. Fujita, N. Mitamura and Y. Murakami: 'Research of new factors affecting rolling contact fatigue life', Proc. World Tribology Congress III, Washington, DC, USA, September 2005, ASME, 1–2.
37. Y. Matsumoto, Y. Murakami and M. Oohori: 'Rolling contact fatigue under water-infiltrated lubrication', in 'Bearing steel technology', (ed. J. M. Beswick), 226–243; 2002, West Conshohocken, PA, ASTM International.
38. H. Uyama, H. Yamada, H. Hidaka and N. Mitamura: 'The effects of hydrogen on microstructural change and surface originated flaking in rolling contact fatigue', *Tribol. Online*, 2011, **6**, (2), 123–132.
39. K. Hiraoka, T. Fujimatsu, N. Tsunekage and A. Yamamoto: 'Generation process observation of micro-structural change in rolling contact fatigue by hydrogen-charged specimens', *Jpn J. Tribol.*, 2007, **52**, (6), 673–683.
40. R. Österlund, O. Vingsbo, L. Vincent and P. Guiraldenq: 'Butterflies in fatigued ball bearings – formation mechanism and structure', *Scand. J. Metall.*, 1982, **11**, 23–32.
41. W. J. Davies and K. L. Day: 'Surface fatigue in ball bearings, roller bearings, and gears in aircraft engines', Proc. Symp. on 'Fatigue in rolling contact', London, UK, March 1963, Institution of Mechanical Engineers, 23–40.
42. Y. Murakami, M. Naka, A. Iwamoto and G. Chatell: 'Long life bearings for automotive alternator applications', Proc. Int. Cong. Exposit., Detroit, MI, USA, February–March 1995, SAE International, 1–14.
43. N. Kino and K. Otani: 'The influence of hydrogen on rolling contact fatigue life and its improvement', *JSAE Rev.*, 2003, **24**, (3), 289–294.
44. K. Tamada and H. Tanaka: 'Occurrence of brittle flaking on bearings used for automotive electrical instruments and auxiliary devices', *Wear*, 1996, **199**, (2), 245–252.
45. J. A. Martin, S. F. Borgese and A. D. Eberhardt: 'Microstructural alterations of rolling bearing steels undergoing cyclic stressing', *Trans. ASME J. Basic Eng.*, 1966, **88**, 555–567.
46. J. L. O'Brien and A. H. King: 'Electron microscopy of stress-induced structural alterations near inclusions in bearing steels', *Trans. ASME J. Basic Eng.*, 1966, **88**, 568–572.
47. J. Buchwald and H. W. Heckel: 'An analysis of microstructural changes in 52100 steel bearings due to cyclic stressing', *Trans. ASM*, 1968, **61**, 750–756.
48. D. McVittie: 'Wind turbine gearbox reliability'; 2006. Seattle, WA, Gear Engineers, Inc. Available from: www.sandia.gov/wind/2006reliability/tuesday/14-brianmcniff.pdf.
49. A. Muroga and H. Saka: 'Analysis of rolling contact fatigued microstructure using focused ion beam sputtering and transmission electron microscopy observation', *Scr. Metall. Mater.*, 1995, **33**, (1), 151–156.
50. H. W. Walton: 'The influence of residual stresses on the susceptibility to hydrogen embrittlement in hardened steel components subjected to rolling contact conditions', Proc. SAE Int. Off-Highway Cong., Las Vegas, NV, USA, March 2002, SAE International, 1–6.
51. NSK: 'Long life bearings for engine accessories', *Motion Control*, Aug. 2004, 1–10.
52. M. Kohara, T. Kawamura and M. Egami: 'Study on mechanism of hydrogen generation from lubricants', *Tribol. T.*, 2006, **49**, (1), 53–60.
53. T. Kawamura and H. Mikami: 'Development of NA103A long-life grease for automotive components', *NTN Tech. Rev.*, 2007, **75**, 116–123.
54. H. Mikami and T. Kawamura: 'Influence of electrical current on bearing flaking life', SAE Technical Paper 2007-01-0113, SAE International, Warrendale, PA, USA, 2007.
55. K. Iso, H. Miyajima, K. Denpou, Y. Toda, M. Yamazaki, M. Naka and Y. Fujita: 'Rolling bearing, rolling bearing for fuel cell, compressor for fuel cell system and fuel cell system', US Patent 7,265,080 B2, 2007.
56. H. Nakashima: 'Trends in materials and heat treatments for rolling bearings', *NTN Tech. Rev.*, 2008, 10–17.
57. S. Tanaka and Y. Murakami: 'Rolling bearing', US Patent 7,435,308 B2, 2008.
58. A. Umeda, T. Shiga and K. Ihata: 'Rolling bearing incorporated in auxiliary device for internal combustion engine', US Patent 7,618,193 B2, 2009.
59. H. Harada and Y. Ono: 'Toroidal continuously variable transmission and method for producing torque transmitting member thereof', US Patent 7,488,270 B2, 2009.
60. J. Rosinski and D. Smurthwaite: 'Troubleshooting wind gearbox problems', *Gear Solut.*, 2010, **8**, 22–33.
61. F. Rasmussen, K. Thomsen and T. J. Larsen: 'The gearbox problem revisited', Risø Fact-Sheet AED-RB-17(en), Risø National Laboratory, Roskilde, DenmarK, 2004. Available from: http://www.windwin.de/images/pdf/riso.pdf.
62. P. J. Tavner, J. Xiang and F. Spinato: 'Reliability analysis for wind turbines', *Wind Energy*, 2007, **10**, (1), 1–18.
63. T. Hamilton: 'A more durable wind turbine', *Technol. Rev.*, Dec. 2009.
64. Northern Power Systems: 'The gearbox problem', Northern Power Systems, Barre, VT, USA, July 2009.
65. J. Broehl: 'Gearbox performance probe sparks legal fears', *Windpower Monthly Mag.*, Mar. 2010.
66. W. Musial, S. Butterfield and B. McNiff: 'Improving wind tubine gearbox reliability', Proc. EWEA 2007 Conf., Milan, Italy, 2007, US Department of Commerce, 1–10.
67. S. E. Thor: Proc. 57th IEA Topical Expert Meet., Jyväskylä, Finland, September 2008. http://www.ieawind.org/Task_11/Proceedings/57_Gearboxes.pdf.
68. R. J. K. Wood, A. S. Bahaj, S. R. Turnock, L. Wang and M. Evans: 'Tribological design constraints of marine renewable energy systems', *Phil. Trans. R. Soc. A: Math. Phys. Eng. Sci.*, 2010, **368**, (1929), 4807–4827.
69. E. J. Terrell, W. M. Needelman and J. P. Kyle: 'Tribological challenges to the system', ASME/STLE Int. Joint Tribology Conf., Memphis, TN, USA, October 2009, ASME/STLE, 26–30.
70. H. Siebert: 'Wind turbines power up with oil', *Lubr. Fluid Power*, Sept./Oct. 2006.
71. A. Heege, Y. Radovcic and J. Betran: 'Fatigue load computation of wind turbine gearboxes by coupled structural, mechanism and aerodynamic analysis', *DEWI Mag.*, Feb. 2006, 61–68.
72. T. Burton, D. Sharpe, N. Jenkins and E. Bossanyi: 'Wind energy handbook'; 2001, New York, John Wiley and Sons.
73. E. Vries: 'Wind turbine gearboxes and the effort to improve their reliability', *Windpower Monthly*, Jun. 2010.
74. A. Olver: 'The mechanism of rolling contact fatigue: an update', *P. I. Mech. Eng. J.-J. Eng.*, 2005, **219**, (5), 313–330.
75. With kind permission from Springer Science+Business Media. R. D. Evans, G. L. Doll, C. H. Hager and J. Y. Howe: 'Influence of steel type on the propensity for tribochemical wear in boundary

lubrication with a wind turbine gear oil', *Tribol. Lett.*, 2010, **38**, 25–32. Figures 3 and 7 respectively.
76. J. Beswick, A. A. Gabelli, S. Ioannides, J. H. Tripp and A. P. Voskamp: 'Rolling bearing life models and steel internal cleanliness', in 'Advances in the production and use of steel with improved internal cleanliness', (ed. J. Mahaney), 12–31; 1999, West Conshohocken, PA, ASTM International.
77. J. A. Eckel, P. C. Glaws, J. O. Wolfe and B. J. Zorc: 'Clean engineered steels - progress at the end of the twentieth century', in 'Advances in the production and use of steel with improved internal cleanliness', (ed. J. Mahaney), 1–12; 1999, West Conshohocken, PA, ASTM International.
78. Y. Murakami and S. Beretta: 'Small defects and inhomogeneities in fatigue strength: experiments, models and statistical implications', *Extremes*, 1999, **2**, (2), 123–147.
79. R. Tricot, J. Monnot and M. Lluansi: 'How microstructural alterations affect fatigue properties of 52100 steel', *Met. Eng. Q.*, 1972, **12**, (2), 39–47.
80. R. S. Hyde: 'Microstructural changes from contact fatigue', in 'ASM handbook', Vol. 19, 'Fatigue and fracture', 1749–1780; 1996, Materials Park, OH, ASM International.
81. F. B. Oswald, E. V. Zaretsky and J. V. Poplawski: 'Interference-fit life factors for roller bearings', *Tribol. T.*, 2009, **52**, (4), 415–426.
82. F. B. Oswald, E. V. Zaretsky and J. V. Poplawski: 'Interference-fit life factors for ball bearings', *Tribol. T.*, 2010, **54**, (1), 1–20.
83. R. D. Evans, G. L. Doll, C. H. Hager and J. Y. Howe: 'Influence of steel type on the propensity for tribochemical wear in boundary lubrication with a wind turbine gear oil', *Tribol. Lett.*, 2010, **38**, (1), 25–32.
84. S. Tanaka, K. Yamamura and M. Oohori: 'Excellent stainless bearing steel (ES1)', *Motion Control*, 2000, **8**, 23–26.
85. J. A. Ciruna and H. J. Szieleit: 'The effect of hydrogen on the rolling contact fatigue life of AISI 52100 and 440C steel balls', *Wear*, 1973, **24**, 107–118.
86. O. Zwirlein and H. Schlicht: 'Rolling contact fatigue mechanisms – accelerated testing versus field performance', in 'Rolling contact fatigue testing of bearing steels', ASTM STP 771, (ed. J. J. C. Hoo), 358–379; 1982, West Conshohocken, PA, ASTM International.
87. A. P. Voskamp: 'Material response to rolling contact loading', *J. Tribol.-T. ASME*, 1985, **107**, 359–366.
88. A. P. Voskamp: 'Fatigue and material response in rolling contact', in 'Bearing steels: into the 21st century', (ed. J. J. C. Hoo *et al.*), 152–166; 1998, West Conshohocken, PA, ASTM International.
89. R. D. Evans, C. H. Hager and R. D. Logsdon: 'Friction and wear performance of candidate surface treatments for wind turbine gearbox bearings in high slip contacts', Proc. ASME/STLE 2009 Int. Joint Tribology Conf., Memphis, TN, USA, October 2009, 491–493.
90. R. Gebauer and S. Ruhl: 'Rolling bearings in wind turbine gearboxes', INA Wälzlager Schaeffler oHG, 2003. Available from: http://www.schaeffler.com/remotemedien/media/_shared_media/library/downloads/wwg_de_us.pdf.
91. TheEngineer: 'New coating for cylindrical roller bearings reduces gearbox failures in wind turbine applications', 2009. Available from: http://www.theengineer.co.uk/news/new-coating-for-cylindrical-roller-bearings-reduces-gearbox-failures-in-wind-turbineapplications/312356.article.
92. Schaeffler: 'Protective materials and coatings for extreme environments', 2010. Available from: http://www.ina.de/content.ina.de/de/press/press-releases/press-details.jsp?id=3358849.
93. J. Tao, T. G. Hughes, H. P. Evans, R. W. Snidle, N. A. Hopkinson, M. Talks and J. M. Starbuck: 'Elastohydrodynamic lubrication analyses of gear tooth surfaces from micropitting tests', *J. Tribol.-T. ASME*, 2003, **125**, 267–274.
94. A. P. Voskamp and E. J. Mittemeijer: 'State of residual stress induced by cyclic rolling contact loading', *Mater. Sci. Technol.*, 1997, **13**, (5), 430–438.
95. F. Sadeghi, B. Jalalahmadi, T. S. Slack, N. Raje and N. K. Arakere: 'A review of rolling contact fatigue', *J. Tribol.-T. ASME*, 2009, **131**, (4), 1–15.
96. G. Lundberg and A. Palmgrem: 'Dynamic capacity of rolling bearings', *Acta Polytech. Scand. Mech. Eng. Ser.*, 1947, **3**, 5–50.
97. R. L. Widner: 'Failures of rolling element bearings: failure analysis and prevention', in 'Metals handbook', 9th edn; 1986, Materials Park, OH, ASM International.
98. N. Tsushima: 'Crack propagation of rolling contact fatigue in ball bearing steel due to tensile strain', *NTN Tech. Rev.*, 2007, 128–139.
99. Reprinted from A. Grabulov, R. Petrov, and H.W. Zandbergen: 'EBSD investigation of the crack initiation and TEM/FIB analyses of the microstructural changes around the cracks formed under rolling contact fatigue (RCF)', *Int. J. Fatigue*, 2010, **32**, 576–583 with permission from Elsevier.
100. K. Furumura, Y. Murakami and T. Abe: 'Development of long life bearing steel for full film lubrication and for poor and contaminated lubrication', *Motion Control*, 1996, **1**, 30–36.
101. A. Kerrigan, J. C. Kuijpers, A. Gabelli and E. Ioannides: 'Cleanliness of bearing steels and fatigue life of rolling contacts', in 'Bearing steel technology – advances and state of the art in bearing steel quality assurance', (ed. J. M. Beswick), 101–106; 2006, West Conshohocken, PA, ASTM International.
102. A. Stiénon, A. Fazekas, J. Y. Buffière, A. Vincent, P. Daguier and F. Merchi: 'A new methodology based on X-ray microtomography to estimate stress concentrations around inclusions in high strength steels', *Mater. Sci. Eng. A*, 2009, **A513**–**A514**, 376–383.
103. K. Hashimoto, T. Fujimatsu, N. Tsunekage, K. Hiraoka, K. Kida and E. C. Santos: 'Study of rolling contact fatigue of bearing steels in relation to various oxide inclusions', *Mater. Des.*, 2011, **32**, (3), 1605–1611.
104. K. Hashimoto, T. Fujimatsu, N. Tsunekage, K. Hiraoka, K. Kida and E. C. Santos: 'Effect of inclusion/matrix interface cavities on internal-fracture-type rolling contact fatigue life', *Mater. Des.*, 2011, **32**, (10), 4980–4985.
105. D. Brooksbank and K. W. Andrews: 'Stress fields around inclusions and their relation to mechanical properties', *J. Iron Steel Inst. (Lond.)*, 1971, **210**, 246–255.
106. D. Ray, L. Vincent, B. Coquillet and P. Guirandenq: 'Hydrogen embrittlement of a stainless ball bearing steel', *Wear*, 1980, **65**, 103–111.
107. A. Vincent, G. Lormand, P. Lamagnère, L. Gosset, D. Girodin, G. Dudragne and R. Fougères: 'From white etching areas formed around inclusions to crack nucleation in bearing steels under rolling contact fatigue', in 'Bearing steels: into the 21st century', (ed. J. J. C. Hoo *et al.*), 109–123; 1998, West Conshohocken, PA, ASTM International.
108. H. Mayer, W. Haydn, R. Schuller, S. Issler and M. Bacher-Höchst: 'Very high cycle fatigue properties of bainitic high carbon–chromium steel under variable amplitude conditions', *Int. J. Fatigue*, 2009, **31**, (8–9), 1300–1308.
109. R. F. Johnson and J. R. Blank: 'Fatigue in rolling contact: some metallurgical aspects', *P. I. Mech. Eng.*, 1963, 95–102.
110. M. Brückner, J. Gegner, A. Grabulov, W. Nierlich and J. Slycke: 'Alternative butterfly formation mechanisms in rolling contact fatigue', Proc. 5th Int. Conf. on 'Very high cycle fatigue', Berlin, Germany, June 2011, 138–151.
111. O. Umezawa and K. Nagai: 'Effects of test temperature on internal fatigue crack generation associated with nonmetallic particles in austenitic steels', *Metall. Mater. Trans. A*, 1998, **29A**, 3017–3028.
112. A. H. King and J. L. O'Brien: 'Microstructural alterations in rolling contact fatigue', Proc. 68th ASTM Annual Meeting on 'Advances in electron metallography', Vol. 6, Lafayette, IN, USA, June 1965, ASTM International, 74–88.
113. K. Böhm, H. Schlicht, O. Zwirlein and R. Eberhard: 'Nonmetallic inclusions and rolling contact fatigue', Proc. ASTM May Committee Week on 'Bearing steels: the rating of nonmetallic inclusions', Boston, MA, USA, May 1974, ASTM, 96–113.
114. K. Hono, M. Ohnuma, M. Murayama, S. Nishida, A. Yoshie and T. Takahashi: 'Cementite decomposition in heavily drawn pearlite steel wire', *Scr. Mater.*, 2001, **44**, 977–983.
115. Reprinted with permission from the *J. ASTM Int.*, **3**, (5). copyright ASTM International, 100 Barr Harbour Drive, West Conshocken, PA 19428.
116. By MATTER, Havovy Cama, released under CC BY-NC-ND 2·0 license. http://core.materials.ac.uk/search/detail.php?id=2626.
117. T. Sakai, B. Lian, M. Takeda, K. Shiozawa, N. Oguma, Y. Ochi, M. Nakajima and T. Nakamura: 'Statistical duplex S-N characteristics of high carbon chromium bearing steel in rotating bending in very high cycle regime', *Int. J. Fatigue*, 2010, **32**, (3), 497–504.
118. M. Shibata: 'Trends of studies on rolling contact fatigue life and recent results', *Koyo Eng. J. (English Edition)*, 2004, 8–13.
119. C. Först, J. Slycke, K. van Vliet and S. Yip: 'Point defect concentrations in metastable Fe-C alloys', *Phys. Rev. Lett.*, 2006, **96**, (17), 175501.
120. Y. Ivanisenko, W. Lojkowski, R. Z. Valiev and H.-J. Fecht: 'The mechanism of formation of nanostructure and dissolution of

cementite in a pearlitic steel during high pressure torsion', *Acta Mater.*, 2003, **51**, (18), 5555–5570.
121. Y. Todaka, M. Umemoto, A. Ohno, M. Suzuki, Y. Kawabata and K. Tsuchiya: 'Dissolution of cementite in carbon steels by ball drop deformation and laser heating', *J. Alloys Compd*, 2007, **434–435**, 497–500.
122. S. Ohsaki, K. Hono, H. Hidaka and S. Takaki: 'Characterization of nanocrystalline ferrite produced by mechanical milling of pearlitic steel', *Scr. Mater.*, 2005, **52**, (4), 271–276.
123. Y. Xu, Z. G. Liu, M. Umemoto and K. Tsuchiya: 'Formation and annealing behavior of nanocrystalline ferrite in Fe–0·89C spheroidite steel produced by ball milling', *Metall. Mater. Trans. A*, 2002, **33A**, 2195–2203.
124. N. Min, W. Li, H. Li and X. Jin: 'Atom probe and mossbauer spectroscopy investigations of cementite dissolution in a cold drawn eutectoid steel', *J. Mater. Sci. Technol.*, 2010, **26**, (9), 776–782.
125. V. Gavriljuk: 'Comment on 'cementite decomposition in heavily drawn pearlite steel wire', *Scr. Mater.*, 2002, **46**, 175–177.
126. A. Taniyama, T. Takayama, M. Arai and T. Hamada: 'Structure analysis of ferrite in deformed pearlitic steel by means of X-ray diffraction method with synchrotron radiation', *Scr. Mater.*, 2004, **51**, (1), 53–58.
127. X. Sauvage, A. Chbihi and X. Quelennec: 'Severe plastic deformation and phase transformations', *J. Phys.: Conf. Ser.*, 2010, **240**, 1–8.
128. J. Ćwiek: 'Hydrogen degradation of high-strength steels', *J. Achiev. Mater. Manuf. Eng.*, 2009, **37**, 193–212.
129. L. Grunberg: 'The formation of hydrogen peroxide on fresh metal surfaces', *Proc. Phys. Soc. Lond. Sect. B*, 1953, **66**, 153–161.
130. T. Imran, B. Jacobson and A. Shariff: 'Quantifying diffused hydrogen in AISI-52100 bearing steel and in silver steel under tribo-mechanical action: Pure rotating bending, sliding–rotating bending, rolling–rotating bending and uni-axial tensile loading', *Wear*, 2006, **261**, 86–95.
131. L. Grunberg, D. T. Jamieson and D. Scott: 'Hydrogen penetration in water-accelerated fatigue of rolling surfaces', *Philos. Mag.*, 1963, **8**, (93), 1553–1568.
132. Y. Matsubara and H. Hamada: 'A novel method to evaluate the influence of hydrogen on fatigue properties of high strength steels', *J. ASTM Int.*, 2006, **3**, (2), 1–14.
133. L. Hong, L. Midan, Z. Tiancheng and C. Wuyang: 'Hydrogen-enhanced dislocation emission, motion and nucleation of hydrogen-induced cracking for steel', *Sci. China Ser. E*, 1997, **40E**, (5), 530–538.
134. S. Fujita, S. Matsuoka, Y. Murakami and G. Marquis: 'Effect of hydrogen on mode II fatigue crack behavior of tempered bearing steel and microstructural changes', *Int. J. Fatigue*, 2010, **32**, (6), 943–951.
135. Y. Murakami and H. Matsunaga: 'The effect of hydrogen on fatigue properties of steels used for fuel cell system', *Int. J. Fatigue*, 2006, **28**, (11), 1509–1520.
136. Y. Murakami, T. Kanezaki, Y. Mine and S. Matsuoka: 'Hydrogen embrittlement mechanism in fatigue of austenitic stainless steels', *Metall. Mater. Trans. A*, 2008, **39A**, (6), 1327–1339.
137. P. Ruo and A. V. Olver: 'Hydrogen in lubricated contact', 1st International Conference - Artificial Intelligence for Industrial Applications, Ostravice, CZ, 19–23 February, 2007, European Marie Curie, 1–7.
138. M. Nagumo, H. Uyama and M. Yoshizawa: 'Accelerated failure in high strength steel by alternating hydrogen-charging potential', *Scr. Mater.*, 2001, **44**, 947–952.
139. D. Scott and H. M. Scott: 'The application of electron microscopy to the study of pitting failure of rolling bearings', European Regional Conference on Electron Microscopy, Delft, The Netherlands, August–September 1960, 539–542.
140. C. D. Beachem: 'A new model for hydrogen-assisted cracking (hydrogen 'embrittlement')', *Metall. Trans. B*, 1972, **3B**, (2), 437–451.
141. H. W. Walton: 'Ubiquitous hydrogen', in 'Heat treating: including steel heat treating in the new millennium', (ed. S. J. Midea and G. D. Pfaffmann), 558–563; 1999, Materials Park, OH, ASM International.
142. M. Nagumo, K. Takai and N. Okuda: 'Nature of hydrogen trapping sites in steels induced by plastic deformation', *J. Alloys Compd*, 1999, **293–295**, 310–316.
143. D. Park, I. S. Maroef, A. Landau and D. L. Olson: 'Retained austenite as a hydrogen trap in steel welds', *Weld. J.*, 2002, 27–35.
144. S. Yamasaki and H. K. D. H. Bhadeshia: 'M_4C_3 precipitation in Fe–C–Mo–V steels and relationship to hydrogen trapping', *Proc. R. Soc. Lond. Ser. A*, 2006, **462**, (2072), 2315–2330.
145. T. Otsuka, H. Hanada, H. Nakashima, K. Sakamoto, M. Hayakawa, K. Hashizume and M. Sugisaki: 'Observation of hydrogen distribution around non-metallic inclusions in steels with tritium microautoradiography', *Fusion Sci. Technol.*, 2005, **48**, (1), 708–711.
146. M. Nagumo, M. Nakamura and K. Takai: 'Hydrogen thermal desorption relevent to delayed-fracture susceptibility of high-strength steels', *Metall. Mater. Trans. A*, 2001, **32A**, 339–347.
147. M. Nagumo: 'Hydrogen related failure of steels – a new aspect', *Mater. Sci. Technol.*, 2004, **20**, 940–950.
148. K. Takai, H. Shoda, H. Suzuki and M. Nagumo: 'Lattice defects dominating hydrogen-related failure of metals', *Acta Mater.*, 2008, **56**, (18), 5158–5167.
149. Copyright (2005) by the American Nuclear Society, La Grange Park, IL, USA. T. Otsuka, H. Hanada, H. Nakashima, K. Sakamoto, M. Hayakawa, K. Hashizume and M. Sugisaki: *Fusion Sci. Technol.*, 2005, **48**, (1), 708–711.
150. R. A. Oriani: 'Hydrogen – the versatile embrittler', *Corrosion*, 1987, **43**, (7), 390–397.
151. H. K. Birnbaum and P. Sofronis: 'Hydrogen-enhanced localized plasticity – a mechanism for hydrogen related failure', *Mater. Sci. Eng. A*, 1994, **A176**, (1–2), 191–202.
152. A. Barnoush and H. Vehoff: 'Recent developments in the study of hydrogen embrittlement: Hydrogen effect on dislocation nucleation', *Acta Mater.*, 2010, **58**, (16), 5274–5285.
153. V. G. Gavriljuk, V. N. Bugaev, Y. N. Petrov, A. V. Tarasenko and B. Z. Yanchitski: 'Hydrogen-induced equilibrium vacancies in fcc iron-base alloys', *Scr. Mater.*, 1996, **34**, (6), 903–907.
154. R. B. McLellan and Z. R. Xu: 'Hydrogen-induced vacancies in the iron lattice', *Scr. Mater.*, 1997, **36**, (10), 1201–1205.
155. Y. Tateyama and T. Ohno: 'Stability and clusterization of hydrogen-vacancy complexes in α-Fe: an ab initio study', *Phys. Rev. B: Condens. Matter*, 2003, **67**, (17), 174105.
156. M. Reichelt, T. E. Weirich, J. Mayer, T. Wolf, J. Loos, P. W. Gold and M. Fajfrowski: 'TEM and nanomechanical studies on tribological surface modifications formed on roller bearings under controlled lubrication conditions', *J. Mater. Sci.*, 2006, **41**, (14), 4543–4553.
157. S. M. Hsu and R. S. Gates: 'Effect of materials on tribochemical reactions between hydrocarbons and surfaces', *J. Phys. D: Appl. Phys.*, 2006, **39**, (15), 3128–3137.
158. T. Sakamoto, H. Uetz, J. Föhl and M. A. Khosrawi: 'The reaction layer formed on steel by additives based on sulphur and phosphorus compounds under conditions of boundary lubrication', *Wear*, 1982, **77**, 139–157.
159. G. T. Y. Wan, H. Lankamp, A. D. Vries and E. Ioannides: 'The effect of extreme pressure (EP) lubricants on the life of rolling element bearings', *P. I. Mech. Eng. J.-J. Eng.*, 1994, **208**, 247–252.
160. J. Fitch: 'How water causes bearing failure', *Mach. Lubr. Mag.*, Jul. 2008. Available from: http://www.machinerylubrication.com/Read/1367/water-bearing-failure.
161. L. J. Taylor and H. A. Spikes: 'Friction-enhancing properties of ZDDP antiwear additive: Part I – friction and morphology of ZDDP reaction films', *Tribol. T.*, 2003, **46**, (3), 303–309.
162. A. Thompson and I. M. Bernstein: 'The role of metallurgical variables in hydrogen-assisted environmental fracture', in 'Advances in corrosion science and technology', (ed. M. G. Fontana *et al.*), 53–175; 1980, New York, Plenum Press.
163. P. Schatzberg: 'Inhibition of water-accelerated rolling-contact fatigue', *J. Lubr. Technol.-T. ASME*, 1971, **70**, 231–233.
164. P. J. L. Fernandes and C. McDuling: 'Surface contact fatigue failures in gears', *Eng. Fail. Anal.*, 1997, **4**, (2), 99–107.
165. Y. S. Kang, R. D. Evans and G. L. Doll: 'Roller-raceway slip simulations of wind turbine gearbox bearings using dynamic bearing model', Proc. STLE/ASME 2010 Int. Joint Tribology Conf., San Francisco, CA, USA, October 2010, ASME, 407–409.
166. P. Johansson, S. Bengtsson and S. Dizdar: 'RCF-testing of selectively densified rollers of p/m materials for gear applications', *Adv. Powder Metall. Particul. Mater.s*, 2002, (Part 5), 180–192.
167. J. Lord and R. Larsson: 'Effects of slide-roll ratio and lubricant properties on elastohydrodynamic lubrication film thickness and traction', *P. I. Mech. Eng. J.-J. Eng.*, 2001, **215**, 301–308.
168. D. M. Nuruzzaman and M. A. A. Sheikh: 'EHL oil film thickness under rolling-sliding contact', *J. Mech. Eng.*, 2007, **38**, 58–60.